

Numerical study of conforming space-time methods for Maxwell's equations

Julia I.M. Hauser¹, Marco Zank²

¹Institut für Wissenschaftliches Rechnen,
Technische Universität Dresden,
Zellescher Weg 25, 01217 Dresden, Germany
`julia.hauser@tu-dresden.de`

²Fakultät für Mathematik, Universität Wien,
Oskar-Morgenstern-Platz 1, 1090 Wien, Austria
`marco.zank@univie.ac.at`

Abstract

Time-dependent Maxwell's equations govern electromagnetics. Under certain conditions, we can rewrite these equations into a partial differential equation of second order, which in this case is the vectorial wave equation. For the vectorial wave, we investigate the numerical application and the challenges in the implementation. For this purpose, we consider a space-time variational setting, i.e. time is just another spatial dimension. More specifically, we apply integration by parts in time as well as in space, leading to a space-time variational formulation with different trial and test spaces. Conforming discretizations of tensor-product type result in a Galerkin–Petrov finite element method that requires a CFL condition for stability. For this Galerkin–Petrov variational formulation, we study the CFL condition and its sharpness. To overcome the CFL condition, we use a Hilbert-type transformation that leads to a variational formulation with equal trial and test spaces. Conforming space-time discretizations result in a new Galerkin–Bubnov finite element method that is unconditionally stable. In numerical examples, we demonstrate the effectiveness of this Galerkin–Bubnov finite element method. Furthermore, we investigate different projections of the right-hand side and their influence on the convergence rates.

This paper is the first step towards a more stable computation and a better understanding of vectorial wave equations in a conforming space-time approach.

1 Introduction

The time-dependent Maxwell's equations and their discretization are required in many electromagnetic applications. One application is the modeling of an electric motor which is governed by the Ampère–Maxwell equation. The Ampère–Maxwell equation relates the time-dependent electric field with the current density and the magnetic field. If the corresponding space-time domain is star-shaped with respect to a ball, then we can rewrite Maxwell's system into the vectorial wave equation. Application of this technique in the static case is investigated in [34]. Extensive studies of the static case can be found not only for analytic methods, but also

for the approximation by finite elements, see e.g. [7], or in a more applied static nonlinear example [19]. Moreover, the quasi-static case is examined, see [6].

However, the complete space-time setting of these equations has been studied in less detail. Most approaches for time-dependent Maxwell's equation are either dealing with the frequency domain, see [28], or using different types of time-stepping methods, see [21, Chapter 12.2]. For the latter, proving stability is delicate. One solution is to stabilize the systems which stem from time-stepping methods. The development of such stabilized methods is an active research field, see e.g. [35] on energy-preserving meshing for FDTD schemes or [4] for the Cole–Cole model which involves polarization. Other classical time-stepping methods are the so-called leapfrog and the Newmark-beta methods, where the first is a special case of the second. Comparison and improvement of these methods can be found in [8]. Another class of time-stepping approaches is locally implicit time integrators, see e.g. [18] and references there.

An alternative to time-stepping methods is a space-time approach. Most approaches apply discontinuous Galerkin methods to Maxwell's equations, see [1, 10, 11, 24, 36] and references there. Note that these methods are non-conforming in general.

In this paper, we derive conforming space-time finite element discretizations for the vectorial wave equation without introducing additional unknowns, i.e. without a reformulation of the vectorial wave equation as a first-order system. The advantage of staying with the second-order formulation and of conforming methods is the need for a smaller number of degrees of freedom compared with first-order formulations or discontinuous Galerkin methods. First, we state the variational formulation for different trial and test spaces, i.e. a Galerkin–Petrov formulation. Second, using the so-called modified Hilbert transformation \mathcal{H}_T , introduced in [31, 39], we present a variational formulation with equal trial and test spaces, i.e. a Galerkin–Bubnov formulation. The main goal of this paper is to derive and describe in detail these two conforming space-time methods, the assembling of the resulting linear systems and their comparison concerning stability and convergence. In more detail, we investigate the Galerkin–Petrov formulation and the corresponding CFL condition. Additionally, we elaborate on a Galerkin–Bubnov formulation using the modified Hilbert transformation, where all necessary mathematical tools are developed. In the end, we compare the results of the conforming Galerkin–Petrov and Galerkin–Bubnov finite element methods concerning their stability and convergence behavior by considering numerical examples. Moreover, we investigate the convergence behavior of both conforming space-time approaches when the right-hand side is approximated by two different projections.

Before we introduce the space-time approach, we derive the vectorial wave equation from Maxwell's equations to get a better understanding of the properties of the equation. We state the main ideas but refer to [16, 33] and references for a more detailed derivation. To derive the vectorial wave equation, we need to rewrite Maxwell's equations using differential forms in a Lipschitz domain $Q \subset \mathbb{R}^4$. Hence, we define the Faraday 2-form $F := e \wedge dt + b$, where e is the 1-form corresponding to the electric field \underline{E} and b the 2-form corresponding to the magnetic flux density \underline{B} . Additionally, we define the Maxwell 2-form $G := h \wedge dt - \tilde{d}$ and the source 3-form $\mathcal{J} := \tilde{j} \wedge dt - \tilde{\rho}$, where h is the 1-form corresponding to the magnetic field \underline{H} , \tilde{d} is the 2-form corresponding to the electric flux density \underline{D} , \tilde{j} is the 2-form corresponding to the given electric current density \underline{j} and $\tilde{\rho}$ is the 3-form corresponding to the given charge

density ρ . Following the derivations in [33], Maxwell's equations allow for the representation

$$\left. \begin{aligned} d F &= 0, \\ d G &= \mathcal{J}, \\ G &= \star^{\epsilon, -\mu^{-1}} F, \end{aligned} \right\} \quad (1)$$

where the four-dimensional exterior derivative d is deployed. Here, the Hodge star operator $\star^{\epsilon, -\mu^{-1}}$ is weighted by ϵ for the components of $(dx^{01}, dx^{02}, dx^{03})^\top$ and by $(-\mu^{-1})$ for the components of $(dx^{23}, dx^{31}, dx^{12})^\top$, considering the Euclidean metric in \mathbb{R}^4 .

Next, we derive the space-time vectorial wave equation from the 4D representation (1) of Maxwell's equations. Since we assume that the domain is star-shaped with respect to a ball, the Poincaré lemma [22, Theorem 4.1] is applicable. Hence, the closed form F is exact and there is a potential \mathcal{A} , which is a 1-form such that $d\mathcal{A} = F$. From this, we also derive the following relations in the Euclidean metric

$$\begin{aligned} \underline{E} &= -\partial_t \underline{A} + \nabla_x A_0, \\ \underline{B} &= \text{curl}_x \underline{A}. \end{aligned}$$

Here, the scalar function A_0 is the time component and the vector-valued function $\underline{A} := (A_1, A_2, A_3)^\top$ is the spatial component of \mathcal{A} . If we insert this result into the second equation of (1), combined with the third of (1), we get the second-order differential equation

$$d \star^{\epsilon, -\mu^{-1}} d\mathcal{A} = \mathcal{J}. \quad (2)$$

We emphasize that there is no uniqueness of the potential \mathcal{A} . Indeed, adding to \mathcal{A} the exterior derivative of any 0-form ϕ results again in a suitable potential $\tilde{\mathcal{A}} = \mathcal{A} + d\phi$ which solves equation (2). This is equivalent to adding the space-time gradient $\nabla_{(t,x)}\phi$ of a function $\phi \in H_0^1(Q)$ to $(A_0, \underline{A})^\top$, with the usual Sobolev space $H_0^1(Q)$. In physics, this is called the *gauge invariance*, which 'is a manifestation of (the) nonobservability of \mathcal{A} ', see [20, p. 676]. To make the potential \mathcal{A} unique, we use gauging. A survey of different gauges can be found in [20]. The choice of the gauge determines the resulting partial differential equation. In this paper, we deploy the Weyl gauge which is also named the temporal gauge, [20]. The Weyl gauge is characterized by choosing $A_0 = 0$, i.e. the component of \mathcal{A} in the time direction is zero. Applying it to (2) results in the vectorial wave equation.

Before we state the vectorial wave equation in terms of the Euclidean metric, we introduce some notation that is used in this paper. First, for $d \in \{2, 3\}$, the spatial bounded Lipschitz domain $\Omega \subset \mathbb{R}^d$ with boundary $\partial\Omega$ has the outward unit normal $\underline{n}_x: \partial\Omega \rightarrow \mathbb{R}^d$. Second, for a given terminal time $T > 0$, we define the space-time cylinder $Q := (0, T) \times \Omega \subset \mathbb{R}^{d+1}$ and its lateral boundary $\Sigma := [0, T] \times \partial\Omega \subset \mathbb{R}^{d+1}$. Next, we fix some notation, which differs for $d = 2$ and $d = 3$. For this purpose, let $\underline{f}: Q \rightarrow \mathbb{R}^d$ be a sufficiently smooth, vector-valued function with components f_ι , $\iota = 1, \dots, d$, and $g: Q \rightarrow \mathbb{R}$ sufficiently smooth, scalar-valued function. We introduce the following notation:

- $d = 2$: We define $\underline{a} \times \underline{b} = a_1 b_2 - a_2 b_1$ for vectors $\underline{a} = (a_1, a_2)^\top, \underline{b} = (b_1, b_2)^\top \in \mathbb{R}^2$, and the spatial curl of \underline{f} by the scalar function $\text{curl}_x \underline{f} = \nabla_x \times \underline{f} = \partial_{x_1} f_2 - \partial_{x_2} f_1$ as well as the spatial curl of g by the vector-valued function $\text{curl}_x g = (\partial_{x_2} g, -\partial_{x_1} g)^\top$.
- $d = 3$: In this case, the spatial curl of \underline{f} is given by the vector-valued function

$$\text{curl}_x \underline{f} = \nabla_x \times \underline{f} = (\partial_{x_2} f_3 - \partial_{x_3} f_2, \partial_{x_3} f_1 - \partial_{x_1} f_3, \partial_{x_1} f_2 - \partial_{x_2} f_1)^\top,$$

where \times denotes the usual cross product of vectors in \mathbb{R}^3 .

With this notation and the Weyl gauge, we rewrite equation (2) into the vectorial wave equation for $d = 2, 3$ simply by inserting the definition of the exterior derivative in the Euclidean metric following [2, Chapter 2]. Hence, we want to find a function $\underline{A}: \overline{Q} \rightarrow \mathbb{R}^d$ such that

$$\left. \begin{aligned} \partial_t (\epsilon \partial_t \underline{A}) + \operatorname{curl}_x (\mu^{-1} \operatorname{curl}_x \underline{A}) &= \underline{j} && \text{in } Q, \\ \underline{A}(0, \cdot) &= \underline{0} && \text{in } \Omega, \\ \partial_t \underline{A}(0, \cdot) &= 0 && \text{in } \Omega, \\ \gamma_t \underline{A} &= 0 && \text{on } \Sigma, \end{aligned} \right\} \quad (3)$$

where γ_t is the tangential trace operator, $\underline{j}: Q \rightarrow \mathbb{R}^d$ is a given current density, $\epsilon: \Omega \rightarrow \mathbb{R}^{d \times d}$ is a given permittivity, and $\mu: \Omega \rightarrow \mathbb{R}$ for $d = 2$ and $\mu: \Omega \rightarrow \mathbb{R}^{3 \times 3}$ for $d = 3$ is a given permeability. However, equation (2) is a four-dimensional equation for a four-dimensional vector potential $(A_0, \underline{A})^\top$. Under the Weyl gauge, the fourth equation in (2) is $\operatorname{div}_x(\epsilon(\partial_t \underline{A})) = -\rho$ in Q . On the other hand, this equation holds as long as $\partial_t \underline{A}$ satisfies the initial condition $\operatorname{div}_x(\epsilon \partial_t \underline{A})(0, \cdot) = -\rho(0, \cdot)$ in Ω , see [16] for more details. So, in case of $\partial_t \underline{A}(0, \cdot) = 0$ in Ω we are limited to examples where $\rho(0, \cdot) = 0$ in Ω . However, using the same technique used for inhomogeneous Dirichlet boundary conditions in finite element methods for the Poisson's equation, see e.g. [13], we can extend the results of this paper to inhomogeneous initial data.

With this knowledge, we give an outline of this paper. In Section 2, we recall well-known function spaces, which are needed to state the trial and test spaces of the variational formulations. In Section 3, we introduce the modified Hilbert transformation which allows for a Galerkin–Bubnov formulation. Then, we state different variational formulations and their properties in Section 4. Section 5 is devoted to the finite element spaces. These approximation spaces are used for the space-time continuous Galerkin finite element discretizations in Section 6, including investigations of a resulting CFL condition. Numerical examples for a two-dimensional spatial domain are presented in Section 7, which show the sharpness of the CFL condition and the different behavior of the numerical solutions when changing the projection of the right-hand side. Finally, we draw conclusions in Section 8.

2 Classical function spaces

For completeness, we recall classical function spaces, see [3, 12, 28, 39] for further details and references. For this purpose, let a bounded Lipschitz domain $D \subset \mathbb{R}^m$ for $m \in \mathbb{N}$ be fixed. We denote by $L^p(D)$, $1 \leq p \leq \infty$, the usual Lebesgue space with its norm $\|\cdot\|_{L^p(D)}$, and by $H^k(D)$, $k \in \mathbb{N}$, the Sobolev space with Hilbertian norm $\|\cdot\|_{H^k(D)}$. Further, the subspace $H_0^1(D) := \{v \in H^1(D) : v|_{\partial D} = 0\} \subset H^1(D)$ is endowed with the Hilbertian norm $\|\cdot\|_{H_0^1(D)} := |\cdot|_{H^1(D)} := \|\nabla_x(\cdot)\|_{L^2(D)}$, which is actually a norm in $H_0^1(D)$ due to the Poincaré inequality. For the interval $D = (0, T)$, we write $L^2(0, T) := L^2((0, T))$, $H^k(0, T) := H^k((0, T))$, and the subspaces

$$\begin{aligned} H_0^1(0, T) &:= \{v \in H^1(0, T) : v(0) = 0\} \subset H^1(0, T), \\ H_0^1(0, T) &:= \{v \in H^1(0, T) : v(T) = 0\} \subset H^1(0, T) \end{aligned}$$

are equipped with the Hilbertian norm $|\cdot|_{H^1(0, T)} := \|\partial_t(\cdot)\|_{L^2(0, T)}$, which again, is actually a norm in $H_0^1(0, T)$ and $H_0^1(0, T)$ due to Poincaré inequalities. By interpolation, we introduce $H_0^s(0, T) := [H_0^1(0, T), L^2(0, T)]_s$ and $H_0^s(0, T) := [H_0^1(0, T), L^2(0, T)]_s$ for $s \in [0, 1]$.

Further, the aforementioned spaces are generalized from real-valued functions $v: \mathbf{D} \rightarrow \mathbb{R}$ to vector-valued functions $v: \mathbf{D} \rightarrow X$ for a Hilbert space X with inner product $(\cdot, \cdot)_X$. In particular, for $X = \mathbb{R}^n$ with $n \in \mathbb{N}$, the space $L^2(\mathbf{D}; \mathbb{R}^n)$ is the usual Lebesgue space for vector-valued functions $\underline{v}: \mathbf{D} \rightarrow \mathbb{R}^n$ endowed with the inner product $(\underline{v}, \underline{w})_{L^2(\mathbf{D})} := (\underline{v}, \underline{w})_{L^2(\mathbf{D}; \mathbb{R}^n)} := \int_{\mathbf{D}} \underline{v}(x) \cdot \underline{w}(x) dx$ for $\underline{v}, \underline{w} \in L^2(\mathbf{D}; \mathbb{R}^n)$ and the induced norm $\|\cdot\|_{L^2(\mathbf{D})} := \|\cdot\|_{L^2(\mathbf{D}; \mathbb{R}^n)} := \sqrt{(\cdot, \cdot)_{L^2(\mathbf{D})}}$.

With this notation, for a bounded Lipschitz domain $\Omega \subset \mathbb{R}^d$ with $d \in \{2, 3\}$, we define the vector-valued Sobolev spaces

$$H(\operatorname{div}; \Omega) := \left\{ \underline{v} \in L^2(\Omega; \mathbb{R}^d) : \operatorname{div}_x \underline{v} \in L^2(\Omega; \mathbb{R}) \right\}$$

endowed with the Hilbertian norm $\|\underline{v}\|_{H(\operatorname{div}; \Omega)} := \left(\|\underline{v}\|_{L^2(\Omega)}^2 + \|\operatorname{div}_x \underline{v}\|_{L^2(\Omega)}^2 \right)^{1/2}$, where div_x is the (distributional) divergence. Similarly, with the (distributional) curl, we set

$$H(\operatorname{curl}; \Omega) := \begin{cases} \{ \underline{v} \in L^2(\Omega; \mathbb{R}^2) : \operatorname{curl}_x \underline{v} \in L^2(\Omega; \mathbb{R}) \}, & d = 2, \\ \{ \underline{v} \in L^2(\Omega; \mathbb{R}^3) : \operatorname{curl}_x \underline{v} \in L^2(\Omega; \mathbb{R}^3) \}, & d = 3, \end{cases}$$

equipped with their natural Hilbertian norm $\|\underline{v}\|_{H(\operatorname{curl}; \Omega)} := \left(\|\underline{v}\|_{L^2(\Omega)}^2 + \|\operatorname{curl}_x \underline{v}\|_{L^2(\Omega)}^2 \right)^{1/2}$.

Next, we introduce the tangential trace operator γ_t for $d \in \{2, 3\}$, see [3], [12, Section 4.3], [14, Theorem 2.11] and [28, Subsection 3.5.3] for details. For this purpose, we denote by $(\cdot)|_{\partial\Omega}$ the usual trace of a function as a linear, surjective mapping from $H^1(\Omega; \mathbb{R}^m)$ onto $H^{1/2}(\partial\Omega; \mathbb{R}^m)$ with $m \in \mathbb{N}$. Here, $H^{1/2}(\partial\Omega; \mathbb{R}^m)$, $m \in \mathbb{N}$, is the fractional-order Sobolev space equipped with the Sobolev–Slobodeckij norm, see [12, Subsection 2.2.2], and $H^{-1/2}(\partial\Omega; \mathbb{R}^m)$ is its dual space. To define the tangential trace operator γ_t , we distinguish two cases:

- $d = 2$: For a function $\underline{w} \in H^1(\Omega; \mathbb{R}^2)$, we define the pointwise trace $\tilde{\gamma}_t \underline{w} = \underline{w}|_{\partial\Omega} \cdot \underline{\tau}_x$, where $\underline{\tau}_x$ is the unit tangent vector satisfying $\underline{\tau}_x \cdot \underline{n}_x = 0$. Then, the continuous mapping $\gamma_t: H(\operatorname{curl}; \Omega) \rightarrow H^{-1/2}(\partial\Omega; \mathbb{R})$ is the unique extension of $\tilde{\gamma}_t$.
- $d = 3$: Analogously, for a function $\underline{w} \in H^1(\Omega; \mathbb{R}^3)$, we set the pointwise trace as the function $\tilde{\gamma}_t \underline{w} = \underline{w}|_{\partial\Omega} \times \underline{n}_x$, and the continuous mapping $\gamma_t: H(\operatorname{curl}; \Omega) \rightarrow H^{-1/2}(\partial\Omega; \mathbb{R}^3)$ as the unique extension of $\tilde{\gamma}_t$.

Having defined the tangential trace operator γ_t for $d \in \{2, 3\}$, we introduce the closed subspace

$$H_0(\operatorname{curl}; \Omega) := \{ \underline{v} \in H(\operatorname{curl}; \Omega) : \gamma_t \underline{v} = 0 \} \subset H(\operatorname{curl}; \Omega)$$

with the Hilbertian norm $\|\cdot\|_{H_0(\operatorname{curl}; \Omega)} := \|\cdot\|_{H(\operatorname{curl}; \Omega)}$. Last, we recall that the set $C_0^\infty(\Omega; \mathbb{R}^d)$ of smooth functions with compact support is dense in $H_0(\operatorname{curl}; \Omega)$ with respect to $\|\cdot\|_{H_0(\operatorname{curl}; \Omega)}$, see [14, Theorem 2.12].

3 Modified Hilbert transformation

In this section, we introduce the modified Hilbert transformation \mathcal{H}_T as developed in [31, 39], and state its main properties, see also [30, 32, 40, 41]. The modified Hilbert transformation acts in time only. Hence, in this section, we consider functions $v: (0, T) \rightarrow \mathbb{R}$, where a generalization to functions in (t, x) is straightforward because of the tensor product structure of the domain Q .

For $v \in L^2(0, T)$, we consider the Fourier series expansion

$$v(t) = \sum_{k=0}^{\infty} v_k \sin\left(\left(\frac{\pi}{2} + k\pi\right) \frac{t}{T}\right), \quad v_k := \frac{2}{T} \int_0^T v(t) \sin\left(\left(\frac{\pi}{2} + k\pi\right) \frac{t}{T}\right) dt,$$

and we define the modified Hilbert transformation \mathcal{H}_T as

$$(\mathcal{H}_T v)(t) = \sum_{k=0}^{\infty} v_k \cos\left(\left(\frac{\pi}{2} + k\pi\right) \frac{t}{T}\right), \quad t \in (0, T). \quad (4)$$

Note that the functions $t \mapsto \sin\left(\left(\frac{\pi}{2} + k\pi\right) \frac{t}{T}\right)$, $k \in \mathbb{N}_0$, form an orthogonal basis of $L^2(0, T)$ and $H_0^1(0, T)$, whereas the functions $t \mapsto \cos\left(\left(\frac{\pi}{2} + k\pi\right) \frac{t}{T}\right)$, $k \in \mathbb{N}_0$, form an orthogonal basis of $L^2(0, T)$ and $H_{,0}^1(0, T)$. Hence, the mapping $\mathcal{H}_T: H_{0,}^s(0, T) \rightarrow H_{,0}^s(0, T)$ is an isomorphism for $s \in [0, 1]$, where the inverse is the $L^2(0, T)$ -adjoint, i.e.

$$(\mathcal{H}_T v, w)_{L^2(0, T)} = (v, \mathcal{H}_T^{-1} w)_{L^2(0, T)} \quad (5)$$

for all $v, w \in L^2(0, T)$. In addition, the relations

$$(v, \mathcal{H}_T v)_{L^2(0, T)} > 0 \quad \text{for } 0 \neq v \in H_{0,}^s(0, T), 0 < s \leq 1, \quad (6)$$

$$\partial_t \mathcal{H}_T v = -\mathcal{H}_T^{-1} \partial_t v \text{ in } L^2(0, T) \quad \text{for } v \in H_{0,}^1(0, T) \quad (7)$$

hold true. For the proofs of these aforementioned properties, we refer to [30, 31, 32, 39, 40, 41]. Furthermore, the modified Hilbert transformation (4) allows a closed representation [31, Lemma 2.8] as Cauchy principal value integral, i.e. for $v \in L^2(0, T)$,

$$(\mathcal{H}_T v)(t) = \text{v.p.} \int_0^T \frac{1}{2T} \left(\frac{1}{\sin \frac{\pi(s+t)}{2T}} + \frac{1}{\sin \frac{\pi(s-t)}{2T}} \right) v(s) ds, \quad t \in (0, T).$$

Further integral representations of \mathcal{H}_T are contained in [32, 41].

4 Space-time variational formulations

In this section, we state space-time variational formulations of the vectorial wave equation (3). For this purpose, we recall a variational setting with different trial and test spaces as well as establish the tools to design a new space-time variational formulation of the vectorial wave equation (3) with equal trial and test spaces. The latter space-time variational formulation is derived by using the modified Hilbert transformation \mathcal{H}_T for the temporal part as introduced in Section 3.

To deploy the existence and uniqueness result of [16] to the stated variational setting, we make the following assumptions, which are assumed for the rest of this work.

Assumption 4.1 ([16, Assumption 1]). *Let the spatial domain $\Omega \subset \mathbb{R}^d$, $d = 2, 3$, be given such that*

- Ω is a bounded Lipschitz domain,
- and $Q := (0, T) \times \Omega$ is star-shaped with respect to a ball B , i.e. the convex hull of B and each point in Q is contained in Q .

Moreover, let \underline{j} , ϵ and μ be given functions, which satisfy:

- The function $\underline{j}: Q \rightarrow \mathbb{R}^d$ is in $L^2(Q; \mathbb{R}^d)$.
- The permittivity $\epsilon \in L^\infty(\Omega; \mathbb{R}^{d \times d})$ is symmetric, and uniformly positive definite, i.e.

$$\operatorname{ess\,inf}_{x \in \Omega} \inf_{0 \neq \xi \in \mathbb{R}^d} \frac{\xi^\top \epsilon(x) \xi}{\xi^\top \xi} > 0.$$

- For $d = 2$, the permeability $\mu \in L^\infty(\Omega; \mathbb{R})$ satisfies

$$\operatorname{ess\,inf}_{x \in \Omega} \mu(x) > 0.$$

For $d = 3$, the permeability $\mu \in L^\infty(\Omega; \mathbb{R}^{3 \times 3})$ is symmetric, and uniformly positive definite, i.e.

$$\operatorname{ess\,inf}_{x \in \Omega} \inf_{0 \neq \xi \in \mathbb{R}^3} \frac{\xi^\top \mu(x) \xi}{\xi^\top \xi} > 0.$$

Note that in Assumption 4.1, the given functions \underline{j} , ϵ and μ are real-valued and that the functions ϵ , μ do not depend on the temporal variable t . Further, to handle the case that Q is not star-shaped with respect to a ball, we introduce the vectorial wave equation (3) in an extended space-time domain \tilde{Q} , which is star-shaped with respect to a ball and fulfills $Q \subset \tilde{Q}$. Here, the functions \underline{j} , ϵ and μ have to be extended appropriately by considering the material, e.g. assuming $\tilde{Q} \setminus \bar{Q}$ is filled with air.

4.1 Different trial and test spaces

In this subsection, we derive a space-time variational formulation of the vectorial wave equation (3), where the trial and test spaces are different. With the aforementioned assumptions on the functions ϵ and μ the function spaces $L^2(\Omega; \mathbb{R}^d)$ and $H_0(\operatorname{curl}; \Omega)$ are endowed with the inner products

$$(\underline{v}, \underline{w})_{L_\epsilon^2(\Omega)} := \int_{\Omega} (\epsilon(x) \underline{v}(x)) \cdot \underline{w}(x) dx, \quad \underline{v}, \underline{w} \in L^2(\Omega; \mathbb{R}^d),$$

and

$$(\underline{v}, \underline{w})_{H_{0,\epsilon,\mu}(\operatorname{curl}; \Omega)} := (\underline{v}, \underline{w})_{L_\epsilon^2(\Omega)} + (\underline{v}, \underline{w})_{H_{0,\mu}(\operatorname{curl}; \Omega)}, \quad \underline{v}, \underline{w} \in H_0(\operatorname{curl}; \Omega),$$

respectively, where

$$(\underline{v}, \underline{w})_{H_{0,\mu}(\operatorname{curl}; \Omega)} := \int_{\Omega} (\mu(x)^{-1} \operatorname{curl}_x \underline{v}(x)) \cdot \operatorname{curl}_x \underline{w}(x) dx, \quad \underline{v}, \underline{w} \in H_0(\operatorname{curl}; \Omega).$$

We denote the induced norms by $\|\cdot\|_{L_\epsilon^2(\Omega)}$, $\|\cdot\|_{H_{0,\epsilon,\mu}(\operatorname{curl}; \Omega)}$ and the seminorm by $|\cdot|_{H_{0,\mu}(\operatorname{curl}; \Omega)} := \sqrt{(\cdot, \cdot)_{H_{0,\mu}(\operatorname{curl}; \Omega)}}$. Further, the norm $\|\cdot\|_{L_\epsilon^2(\Omega)}$ is equivalent to $\|\cdot\|_{L^2(\Omega)}$ as well as the norm $\|\cdot\|_{H_{0,\epsilon,\mu}(\operatorname{curl}; \Omega)}$ is equivalent to $\|\cdot\|_{H_0(\operatorname{curl}; \Omega)}$.

Next, we define the space-time Sobolev spaces, which are used for the variational formulation. We consider

$$H_{0,0}^{\operatorname{curl};1}(Q) := L^2(0, T; H_0(\operatorname{curl}; \Omega)) \cap H_0^1(0, T; L^2(\Omega; \mathbb{R}^d)), \quad (8)$$

$$H_{0,0}^{\operatorname{curl};1}(Q) := L^2(0, T; H_0(\operatorname{curl}; \Omega)) \cap H_0^1(0, T; L^2(\Omega; \mathbb{R}^d)), \quad (9)$$

which are endowed with the Hilbertian norm

$$\begin{aligned} |\underline{v}|_{H^{\text{curl};1}(Q)} &:= \|\underline{v}\|_{H_{0,0}^{\text{curl};1}(Q)} := \|\underline{v}\|_{H_{0,0}^{\text{curl};1}(Q)} \\ &:= \left(\int_0^T \|\partial_t \underline{v}(t, \cdot)\|_{L_\varepsilon^2(\Omega)}^2 dt + \int_0^T |\underline{v}(t, \cdot)|_{H_{0,\mu}(\text{curl};\Omega)}^2 dt \right)^{1/2}. \end{aligned}$$

Note that $|\cdot|_{H^{\text{curl};1}(Q)}$ is actually a norm in $H_{0,0}^{\text{curl};1}(Q)$ and $H_{0,0}^{\text{curl};1}(Q)$, since the Poincaré inequality

$$\|\underline{v}\|_{L^2(Q)} \leq \frac{2T}{\pi} \|\partial_t \underline{v}\|_{L^2(Q)}$$

holds true for all $\underline{v} \in H_0^1(0, T; L^2(\Omega; \mathbb{R}^d))$ and for all $\underline{v} \in H_0^1(0, T; L^2(\Omega; \mathbb{R}^d))$. This Poincaré inequality follows from

$$\|\underline{v}\|_{L^2(Q)}^2 = \sum_{\iota=1}^d \int_{\Omega} \|v_{\iota}(\cdot, x)\|_{L^2(0,T)}^2 dx \leq \frac{4T^2}{\pi^2} \sum_{\iota=1}^d \int_{\Omega} \|\partial_t v_{\iota}(\cdot, x)\|_{L^2(0,T)}^2 dx = \frac{4T^2}{\pi^2} \|\partial_t \underline{v}\|_{L^2(Q)}^2$$

for all $\underline{v} = (v_1, \dots, v_d)^\top$ with $\underline{v} \in H_0^1(0, T; L^2(\Omega; \mathbb{R}^d))$ or $\underline{v} \in H_0^1(0, T; L^2(\Omega; \mathbb{R}^d))$, where [39, Lemma 3.4.5] is applied.

With these space-time Sobolev spaces, we motivate a space-time variational formulation of the vectorial wave equation (3). For this purpose, we multiply the vectorial wave equation (3) by a test function \underline{v} , integrate over the space-time domain Q and then use integration by parts with respect to space and time, resulting in the space-time variational formulation: Find $\underline{A} \in H_{0,0}^{\text{curl};1}(Q)$ such that

$$- (\varepsilon \partial_t \underline{A}, \partial_t \underline{v})_{L^2(Q)} + (\mu^{-1} \text{curl}_x \underline{A}, \text{curl}_x \underline{v})_{L^2(Q)} = (\underline{j}, \underline{v})_{L^2(Q)} \quad (10)$$

for all $\underline{v} \in H_{0,0}^{\text{curl};1}(Q)$.

Note that the first initial condition $\underline{A}(0, \cdot) = 0$ is fulfilled in the strong sense, whereas the second initial condition $\partial_t \underline{A}(0, \cdot) = 0$ is incorporated in a weak sense in the right side of (10). On the other hand, the boundary condition $\gamma_t \underline{A} = 0$ is satisfied in the strong sense with $\underline{A}(t, \cdot) \in H_0(\text{curl}; \Omega)$ for almost all $t \in (0, T)$.

The unique solvability of the variational formulation (10) is proven in [17], [15, Theorem 3.8], and in [16] as a special case of Theorem 2, which is summarized in the next theorem.

Theorem 4.2. *Let Assumption 4.1 be satisfied. Then, a unique solution $\underline{A} \in H_{0,0}^{\text{curl};1}(Q)$ of the variational formulation (10) exists and the stability estimate*

$$|\underline{A}|_{H^{\text{curl};1}(Q)} \leq T \|\underline{j}\|_{L^2(Q)}$$

holds true.

Note that the trial and test spaces of the variational formulation (10) are different. To get equal trial and test spaces, the modified Hilbert transformation \mathcal{H}_T of Section 3 is used, which is investigated in the next subsection.

4.2 Equal trial and test spaces

The goal of this subsection is to state a space-time variational formulation of the vectorial wave equation (3) with equal trial and test spaces. For this purpose, we extend the definition of the modified Hilbert transformation \mathcal{H}_T of Section 3 to the vector-valued functions in $H_{0,0}^{\text{curl},1}(Q)$ and $H_{0,0}^{\text{curl},1}(Q)$, where the extension is denoted again by \mathcal{H}_T . More precisely, we define the mapping $\mathcal{H}_T: L^2(Q; \mathbb{R}^d) \rightarrow L^2(Q; \mathbb{R}^d)$ by

$$(\mathcal{H}_T \underline{v})(t, x) := \sum_{i=-\infty}^{\infty} \sum_{k=0}^{\infty} v_{i,k} \cos \left(\left(\frac{\pi}{2} + k\pi \right) \frac{t}{T} \right) \underline{\varphi}_i(x), \quad (t, x) \in Q, \quad (11)$$

where the given function $\underline{v} \in L^2(Q; \mathbb{R}^d)$ is represented by

$$\underline{v}(t, x) = \sum_{i=-\infty}^{\infty} \sum_{k=0}^{\infty} v_{i,k} \sin \left(\left(\frac{\pi}{2} + k\pi \right) \frac{t}{T} \right) \underline{\varphi}_i(x), \quad (t, x) \in Q. \quad (12)$$

Here, the set $\{\underline{\varphi}_i \in H_0(\text{curl}; \Omega) : i \in \mathbb{Z}\}$ is

- an orthonormal basis of $L^2(\Omega; \mathbb{R}^d)$ with respect to $(\cdot, \cdot)_{L^2(\Omega)}$,
- an orthogonal basis of $H_0(\text{curl}; \Omega)$ with respect to $(\cdot, \cdot)_{H_{0,\epsilon,\mu}(\text{curl}; \Omega)}$, and
- orthogonal with respect to $(\cdot, \cdot)_{H_{0,\mu}(\text{curl}; \Omega)}$,

where we refer to [16, Subsection 1.1.1] and [3, Subsection 8.3.1.2] for the construction of such a basis. The inverse operator $\mathcal{H}_T^{-1}: L^2(Q; \mathbb{R}^d) \rightarrow L^2(Q; \mathbb{R}^d)$ is defined by

$$(\mathcal{H}_T^{-1} \underline{w})(t, x) = \sum_{i=-\infty}^{\infty} \sum_{k=0}^{\infty} w_{i,k} \sin \left(\left(\frac{\pi}{2} + k\pi \right) \frac{t}{T} \right) \underline{\varphi}_i(x), \quad (t, x) \in Q,$$

where the given function $\underline{w} \in L^2(Q; \mathbb{R}^d)$ is represented by

$$\underline{w}(t, x) = \sum_{i=-\infty}^{\infty} \sum_{k=0}^{\infty} w_{i,k} \cos \left(\left(\frac{\pi}{2} + k\pi \right) \frac{t}{T} \right) \underline{\varphi}_i(x), \quad (t, x) \in Q. \quad (13)$$

Next, we prove properties of this definition of the modified Hilbert transformation \mathcal{H}_T . These properties are then used for the derivation of a Galerkin–Bubnov method for the space-time variational formulation of the vectorial wave equation (3). Recall the definition of the vector-valued space-time Sobolev spaces $H_{0,0}^{\text{curl},1}(Q)$, $H_{0,0}^{\text{curl},1}(Q)$ defined in (8), (9).

Lemma 4.3. *The mapping $\mathcal{H}_T: H_{0,0}^{\text{curl},1}(Q) \rightarrow H_{0,0}^{\text{curl},1}(Q)$ is bijective and norm preserving, i.e. $|\underline{v}|_{H^{\text{curl},1}(Q)} = |\mathcal{H}_T \underline{v}|_{H^{\text{curl},1}(Q)}$ for all $\underline{v} \in H_{0,0}^{\text{curl},1}(Q)$.*

Proof. We follow the arguments in [39, Subsection 3.4.5]. Let $\underline{v} \in H_{0,0}^{\text{curl},1}(Q)$ be fixed with the Fourier representations (12). The relation $\mathcal{H}_T \underline{v} \in H_{0,0}^{\text{curl},1}(Q)$ and the bijectivity follow by definition. To prove the equality $|\underline{v}|_{H^{\text{curl},1}(Q)} = |\mathcal{H}_T \underline{v}|_{H^{\text{curl},1}(Q)}$, we use the representations (11), (12) to calculate the functions $\partial_t \mathcal{H}_T \underline{v}$, $\text{curl}_x \mathcal{H}_T \underline{v}$, $\partial_t \underline{v}$, $\text{curl}_x \underline{v}$ as Fourier series. Plugging them into the norms $|\underline{v}|_{H^{\text{curl},1}(Q)}$, $|\mathcal{H}_T \underline{v}|_{H^{\text{curl},1}(Q)}$, and deploying the orthogonality relations of the basis $\{\underline{\varphi}_i \in H_0(\text{curl}; \Omega) : i \in \mathbb{Z}\}$ yield the assertion. \square

As \mathcal{H}_T acts only with respect to time, the properties (5), (7) of Section 3 remain valid. For completeness, we prove the following lemma.

Lemma 4.4. *The relations*

$$(\epsilon \mathcal{H}_T \underline{v}, \underline{w})_{L^2(Q)} = (\epsilon \underline{v}, \mathcal{H}_T^{-1} \underline{w})_{L^2(Q)} \quad (14)$$

for all $\underline{v} \in L^2(Q; \mathbb{R}^d)$ and $\underline{w} \in L^2(Q; \mathbb{R}^d)$, and

$$\mathcal{H}_T^{-1} \partial_t \underline{v} = -\partial_t \mathcal{H}_T \underline{v} \quad (15)$$

in $L^2(Q; \mathbb{R}^d)$ for all $\underline{v} \in H_0^1(0, T; L^2(\Omega; \mathbb{R}^d))$ are true.

Proof. First, we prove property (14). Let $\underline{v} \in L^2(Q; \mathbb{R}^d)$ and $\underline{w} \in L^2(Q; \mathbb{R}^d)$ be fixed with the Fourier representations (12) and (13), respectively. Using the orthogonality properties of the involved basis functions and the symmetry of ϵ as stated in Assumption 4.1 yield

$$(\epsilon \mathcal{H}_T \underline{v}, \underline{w})_{L^2(Q)} = \frac{T}{2} \sum_{i=-\infty}^{\infty} \sum_{k=0}^{\infty} v_{i,k} w_{i,k} = (\epsilon \underline{v}, \mathcal{H}_T^{-1} \underline{w})_{L^2(Q)},$$

and thus, property (14).

Second, to prove property (15), fix again $\underline{v} \in H_0^1(0, T; L^2(\Omega; \mathbb{R}^d))$ with the Fourier representations (12), which converges in $H_0^1(0, T; L^2(\Omega; \mathbb{R}^d))$. Thus, the Fourier series

$$\mathcal{H}_T^{-1} \partial_t \underline{v}(t, x) = \frac{1}{T} \sum_{i=-\infty}^{\infty} \sum_{k=0}^{\infty} v_{i,k} \left(\frac{\pi}{2} + k\pi \right) \sin \left(\left(\frac{\pi}{2} + k\pi \right) \frac{t}{T} \right) \underline{\varphi}_i(x), \quad (t, x) \in Q,$$

is convergent with respect to $L^2(Q; \mathbb{R}^d)$. Analogously, as the Fourier series (11) converges in $H_0^1(0, T; L^2(\Omega; \mathbb{R}^d))$, the series

$$\partial_t \mathcal{H}_T \underline{v}(t, x) = -\frac{1}{T} \sum_{i=-\infty}^{\infty} \sum_{k=0}^{\infty} v_{i,k} \left(\frac{\pi}{2} + k\pi \right) \sin \left(\left(\frac{\pi}{2} + k\pi \right) \frac{t}{T} \right) \underline{\varphi}_i(x), \quad (t, x) \in Q,$$

is also convergent in $L^2(Q; \mathbb{R}^d)$. Comparing these Fourier representations gives the equality $\mathcal{H}_T^{-1} \partial_t \underline{v} = -\partial_t \mathcal{H}_T \underline{v}$ in $L^2(Q; \mathbb{R}^d)$. \square

Last, we need the following result.

Lemma 4.5. *For $\underline{v} \in L^2(Q; \mathbb{R}^d)$, the equality*

$$\mathcal{H}_T(\epsilon \underline{v}) = \epsilon \mathcal{H}_T \underline{v} \quad \text{in } L^2(Q; \mathbb{R}^d)$$

holds true.

Proof. Let $\underline{v} \in L^2(Q; \mathbb{R}^d)$ be a fixed function. With the normalized eigenfunction $\psi_k(t) = \sqrt{\frac{2}{T}} \sin \left(\left(\frac{\pi}{2} + k\pi \right) \frac{t}{T} \right)$, we have the representations

$$\begin{aligned} (\epsilon \underline{v})(t, x) &= \sum_{i=-\infty}^{\infty} \sum_{k=0}^{\infty} (\epsilon \underline{v}, \psi_k \underline{\varphi}_i)_{L^2(Q)} \psi_k(t) \underline{\varphi}_i(x), \quad (t, x) \in Q, \\ \epsilon(x) \underline{v}(t, x) &= \sum_{i=-\infty}^{\infty} \sum_{k=0}^{\infty} (\epsilon \underline{v}, \psi_k \underline{\varphi}_i)_{L^2(Q)} \psi_k(t) \epsilon(x) \underline{\varphi}_i(x), \quad (t, x) \in Q, \end{aligned}$$

which lead to the equality

$$\forall k \in \mathbb{N}_0 : \sum_{i=-\infty}^{\infty} (\epsilon \underline{v}, \psi_k \underline{\varphi}_i)_{L^2(Q)} \underline{\varphi}_i(x) = \sum_{i=-\infty}^{\infty} (\epsilon \underline{v}, \psi_k \underline{\varphi}_i)_{L^2(Q)} \epsilon(x) \underline{\varphi}_i(x)$$

for almost all $x \in \Omega$. Then we derive

$$\begin{aligned} \epsilon(x) (\mathcal{H}_T \underline{v})(t, x) &= \sqrt{\frac{T}{2}} \sum_{k=0}^{\infty} \cos\left(\left(\frac{\pi}{2} + k\pi\right) \frac{t}{T}\right) \sum_{i=-\infty}^{\infty} (\epsilon \underline{v}, \psi_k \underline{\varphi}_i)_{L^2(Q)} \epsilon(x) \underline{\varphi}_i(x) \\ &= \sqrt{\frac{T}{2}} \sum_{k=0}^{\infty} \cos\left(\left(\frac{\pi}{2} + k\pi\right) \frac{t}{T}\right) \sum_{i=-\infty}^{\infty} (\epsilon \underline{v}, \psi_k \underline{\varphi}_i)_{L^2(Q)} \underline{\varphi}_i(x) = \mathcal{H}_T(\epsilon \underline{v})(t, x) \end{aligned}$$

for almost all $(t, x) \in Q$, and hence, the assertion. \square

Next, we derive the Galerkin–Bubnov formulation. With the mapping $\mathcal{H}_T: H_{0,0}^{\text{curl};1}(Q) \rightarrow H_{0,0}^{\text{curl};1}(Q)$, the variational formulation (10) is equivalent to:

Find $\underline{A} \in H_{0,0}^{\text{curl};1}(Q)$ such that

$$-(\epsilon \partial_t \underline{A}, \partial_t \mathcal{H}_T \underline{v})_{L^2(Q)} + (\mu^{-1} \text{curl}_x \underline{A}, \text{curl}_x \mathcal{H}_T \underline{v})_{L^2(Q)} = (\underline{j}, \mathcal{H}_T \underline{v})_{L^2(Q)} \quad (16)$$

for all $\underline{v} \in H_{0,0}^{\text{curl};1}(Q)$.

We rewrite the variational formulation (16) using the properties (14), (15) to get:

Find $\underline{A} \in H_{0,0}^{\text{curl};1}(Q)$ such that

$$(\epsilon \mathcal{H}_T \partial_t \underline{A}, \partial_t \underline{v})_{L^2(Q)} + (\mu^{-1} \text{curl}_x \underline{A}, \text{curl}_x \mathcal{H}_T \underline{v})_{L^2(Q)} = (\underline{j}, \mathcal{H}_T \underline{v})_{L^2(Q)} \quad (17)$$

for all $\underline{v} \in H_{0,0}^{\text{curl};1}(Q)$, where also Lemma 4.5 is applied. The variational formulation (17) has a unique solution, as the equivalent variational formulation (10) is uniquely solvable, see Theorem 4.2, and due to the fact that $\mathcal{H}_T: H_{0,0}^{\text{curl};1}(Q) \rightarrow H_{0,0}^{\text{curl};1}(Q)$ is an isometry, see Lemma 4.3.

5 Finite element spaces

As both variational formulations, the Galerkin–Petrov formulation (10) and the Galerkin–Bubnov formulation (17), are uniquely solvable, we investigate the discrete counterparts of these formulations. For that purpose, we first introduce the finite element spaces, which are used for discretizations of the variational formulations (10) and (17). For comparison reasons, we aim at a similar notation as in [16, Subsection 3.1], where, however, piecewise quadratic instead of piecewise linear functions are used for the temporal discretizations.

Let us start with the spatial discretization. In this section, we assume that the bounded Lipschitz domain $\Omega \subset \mathbb{R}^d$ is polygonal for $d = 2$, or polyhedral for $d = 3$. Let $\nu \in \mathbb{N}_0$ be the refinement level and $(\mathcal{T}_\nu^x)_{\nu \in \mathbb{N}_0}$ the corresponding mesh sequence of admissible decompositions \mathcal{T}_ν^x of the spatial domain Ω . On each level ν we decompose the spatial domain Ω into $N^x := N_\nu^x$ triangles ($d = 2$) or tetrahedra ($d = 3$) denoted by $\omega_\iota \subset \mathbb{R}^d$ for $\iota = 1, \dots, N^x$, satisfying $\overline{\Omega} = \bigcup_{\iota=1}^{N^x} \overline{\omega}_\iota$. Note that also other types of elements ω_ι , e.g. rectangles ($d = 2$), are possible.

We emphasize that we define the local mesh sizes by $h_{x,\iota} = \left(\int_{\omega_\iota} dx\right)^{1/d}$, $\iota = 1, \dots, N^x$, since

this particular choice occurs in the context of the CFL condition of the proposed Galerkin–Petrov method. Further, we define $h_x := h_{x,\max}(\mathcal{T}_\nu^x) := \max_{\ell=1,\dots,N^x} h_{x,\ell}$, and $h_{x,\min}(\mathcal{T}_\nu^x) := \min_{\ell=1,\dots,N^x} h_{x,\ell}$.

For the investigations of CFL conditions, we consider for the rest of the paper a sequence $(\mathcal{T}_\nu^x)_{\nu \in \mathbb{N}_0}$, satisfying a shape-regularity and a global quasi-uniformity. As these terms are not used in a uniform manner, we recall their definition. The mesh sequence $(\mathcal{T}_\nu^x)_{\nu \in \mathbb{N}_0}$ is

- shape-regular if $\exists c_F > 0 : \forall \nu \in \mathbb{N}_0 : \forall \omega \in \mathcal{T}_\nu^x : \sup_{x,y \in \bar{\omega}} \|x - y\|_2 \leq c_F r_\omega$,
- globally quasi-uniform if $\exists c_G \geq 1 : \forall \nu \in \mathbb{N}_0 : \frac{h_{x,\max}(\mathcal{T}_\nu^x)}{h_{x,\min}(\mathcal{T}_\nu^x)} \leq c_G$.

Here, $r_\omega > 0$ is the inradius of the element ω , and $\|x - y\|_2$ is the Euclidean distance of the points x, y in \mathbb{R}^d . The constant c_F influences the conditional stability, namely a CFL condition. To derive this CFL condition, we also need an inverse inequality for the spatial curl operator. The inverse inequality on the other hand is affected by the global quasi-uniformity for finite elements in $H(\text{curl}; \Omega)$.

With these conditions on the spatial mesh in mind, we introduce three spatial approximation spaces of vector-valued type, see [12, Section 19.2], [25, Section 3.5.1] or [28, Section 5.5] for more details. For this purpose, for $p \in \mathbb{N}_0$, $n \in \{1, 2, 3\}$ and $K \subset \mathbb{R}^n$, the polynomials of total degree p are denoted by $\mathbb{P}_n^p(K)$. First, we define the space of vector-valued piecewise constant functions

$$S_d^0(\mathcal{T}_\nu^x) := \left\{ \underline{v}_{h_x} \in L^2(\Omega; \mathbb{R}^d) : \forall \omega \in \mathcal{T}_\nu^x : \underline{v}_{h_x}|_\omega \in \mathbb{P}_d^0(\omega)^d \right\} = \text{span}\{\underline{\psi}_\ell^0\}_{\ell=1}^{N_x^0},$$

where the N_x^0 basis functions $\underline{\psi}_\ell^0$ are the componentwise characteristic functions with respect to the spatial elements. Second, we set the lowest-order Raviart–Thomas finite element space by

$$\mathcal{RT}^0(\mathcal{T}_\nu^x) := \left\{ \underline{v}_{h_x} \in H(\text{div}; \Omega) : \forall \omega \in \mathcal{T}_\nu^x : \underline{v}_{h_x}|_\omega \in \mathcal{RT}^0(\omega) \right\} = \text{span}\{\underline{\psi}_\ell^{\mathcal{RT}}\}_{\ell=1}^{N_x^{\mathcal{RT}}},$$

where the $N_x^{\mathcal{RT}}$ basis functions $\underline{\psi}_\ell^{\mathcal{RT}}$ are attached to the edges for $d = 2$ and the faces for $d = 3$ of the spatial mesh \mathcal{T}_ν^x and

$$\mathcal{RT}^0(\omega) := \left\{ \underline{P} \in \mathbb{P}_d^1(\omega)^d : \forall x \in \omega : \underline{P}(x) = \underline{a} + bx \text{ with } \underline{a} \in \mathbb{R}^d, b \in \mathbb{R} \right\}$$

is the local polynomial space for $\omega \in \mathcal{T}_\nu^x$, see [12, Section 14.1]. Last, we introduce the lowest-order Nédélec finite element space of the first kind by

$$\mathcal{N}_1^0(\mathcal{T}_\nu^x) := \left\{ \underline{v}_{h_x} \in H(\text{curl}; \Omega) : \forall \omega \in \mathcal{T}_\nu^x : \underline{v}_{h_x}|_\omega \in \mathcal{N}_1^0(\omega) \right\},$$

and its subspace having zero tangential trace by

$$\mathcal{N}_{1,0}^0(\mathcal{T}_\nu^x) := \mathcal{N}_1^0(\mathcal{T}_\nu^x) \cap H_0(\text{curl}; \Omega) = \text{span}\{\underline{\psi}_\ell^{\mathcal{N}}\}_{\ell=1}^{N_x^{\mathcal{N}}},$$

where the $N_x^{\mathcal{N}}$ basis functions $\underline{\psi}_\ell^{\mathcal{N}}$ are attached to the edges of the spatial mesh \mathcal{T}_ν^x , and the local polynomial spaces for $\omega \in \mathcal{T}_\nu^x$ are given by

$$\mathcal{N}_1^0(\omega) := \left\{ \underline{P} \in \mathbb{P}_2^1(\omega)^2 : \forall (x_1, x_2) \in \omega : \underline{P}(x_1, x_2) = \underline{a} + b \cdot (-x_2, x_1)^\top \text{ with } \underline{a} \in \mathbb{R}^2, b \in \mathbb{R} \right\}$$

for $d = 2$, and

$$\mathcal{N}_1^0(\omega) := \left\{ \underline{P} \in \mathbb{P}_3^1(\omega)^3 : \forall x \in \omega : \underline{P}(x) = \underline{a} + \underline{b} \times x \text{ with } \underline{a} \in \mathbb{R}^3, \underline{b} \in \mathbb{R}^3 \right\}$$

for $d = 3$, see [12, Section 15.1].

Next, we investigate temporal finite element spaces. For this purpose, we consider a sequence of meshes $\{\mathcal{T}_\alpha^t\}_{\alpha \in \mathbb{N}_0}$ in time. Here, $\alpha \in \mathbb{N}_0$ is the level of refinement and $\mathcal{T}_\alpha^t = \{\tau_l\}_{l=1}^{N_\alpha^t}$ is the mesh defined by the decomposition

$$0 = t_0 < t_1 < \dots < t_{N_\alpha^t-1} < t_{N_\alpha^t} = T$$

of the time interval $(0, T)$, where $N_\alpha^t =: N^t$ is the number of temporal elements $\tau_l = (t_{l-1}, t_l) \subset \mathbb{R}$, $l = 1, \dots, N^t$, with mesh sizes $h_{t,l} = t_l - t_{l-1}$, $l = 1, \dots, N^t$, and $h_t := \max_{l=1, \dots, N^t} h_{t,l}$. First, the space of piecewise constant functions in time is given by

$$S^0(\mathcal{T}_\alpha^t) := \left\{ v_{h_t} \in L^2(0, T) : \forall l \in \{1, \dots, N^t\} : v_{h_t}|_{\tau_l} \in \mathbb{P}_1^0(\tau_l) \right\} = \text{span}\{\varphi_l^0\}_{l=1}^{N^t}$$

with the elementwise characteristic functions φ_l^0 as basis functions. Second, we write the space of piecewise linear, globally continuous functions as

$$S^1(\mathcal{T}_\alpha^t) := \left\{ v_{h_t} \in C[0, T] : \forall l \in \{1, \dots, N^t\} : v_{h_t}|_{\overline{\tau_l}} \in \mathbb{P}_1^1(\overline{\tau_l}) \right\} = \text{span}\{\varphi_l^1\}_{l=1}^{N^t},$$

where the hat function φ_l^1 is related to t_l , i.e. $\varphi_l^1(t_k) = 0$ for $k \neq l$ and $\varphi_l^1(t_l) = 1$. As we need also approximation spaces that incorporate initial or terminal conditions, we define the subspace

$$S_{0,}^1(\mathcal{T}_\alpha^t) := S^1(\mathcal{T}_\alpha^t) \cap H_{0,}^1(0, T) = \text{span}\{\varphi_l^1\}_{l=1}^{N^t},$$

fulfilling the homogeneous initial condition, and the subspace

$$S_{,0}^1(\mathcal{T}_\alpha^t) := S^1(\mathcal{T}_\alpha^t) \cap H_{,0}^1(0, T) = \text{span}\{\varphi_l^1\}_{l=0}^{N^t-1},$$

satisfying the homogeneous terminal condition.

With the spatial and temporal approximation spaces, we introduce the conforming subspaces

$$S_{0,}^1(\mathcal{T}_\alpha^t) \otimes \mathcal{N}_{1,0}^0(\mathcal{T}_\nu^x) \subset H_{0,0}^{\text{curl};1}(Q), \quad (18)$$

$$S_{,0}^1(\mathcal{T}_\alpha^t) \otimes \mathcal{N}_{1,0}^0(\mathcal{T}_\nu^x) \subset H_{0,;0}^{\text{curl};1}(Q), \quad (19)$$

see (8), (9), where \otimes denotes the Hilbert tensor-product. Thus, these space-time approximation spaces are related to the space-time mesh $\{\tau_l \times \omega_\iota : l = 1, \dots, N^t, \iota = 1, \dots, N^x\}$. In other words, the space-time cylinder $Q \subset \mathbb{R}^{d+1}$ is decomposed into $N^t \cdot N^x$ space-time elements $\tau_l \times \omega_\iota \subset \mathbb{R}^{d+1}$ for $l = 1, \dots, N^t, \iota = 1, \dots, N^x$.

Last, to approximate the right-hand side of the vectorial wave equation (3), we consider two different $L^2(Q)$ projections of $\underline{j} \in L^2(Q; \mathbb{R}^d)$. In Section 7 on the numerical results we investigate the influence of the two types of projection on the convergence rates. Let us take a look at the definition of the projections for a given $\underline{g} \in L^2(Q; \mathbb{R}^d)$. First, the projection onto the space of piecewise constant functions $\Pi_h^0 : L^2(Q; \mathbb{R}^d) \rightarrow S^0(\mathcal{T}_\alpha^t) \otimes S_d^0(\mathcal{T}_\nu^x)$ is defined as solution $\Pi_h^0 \underline{g} \in S^0(\mathcal{T}_\alpha^t) \otimes S_d^0(\mathcal{T}_\nu^x)$ such that

$$(\Pi_h^0 \underline{g}, \underline{w}_h)_{L^2(Q)} = (\underline{g}, \underline{w}_h)_{L^2(Q)} \quad (20)$$

for all $\underline{w}_h \in S^0(\mathcal{T}_\alpha^t) \otimes S_d^0(\mathcal{T}_\nu^x)$. Second, the projection onto the space of piecewise linear functions in time and Raviart–Thomas functions in space $\Pi_h^{\mathcal{RT},1}: L^2(Q; \mathbb{R}^d) \rightarrow S^1(\mathcal{T}_\alpha^t) \otimes \mathcal{RT}^0(\mathcal{T}_\nu^x)$ is given as solution $\Pi_h^{\mathcal{RT},1} \underline{g} \in S^1(\mathcal{T}_\alpha^t) \otimes \mathcal{RT}^0(\mathcal{T}_\nu^x)$ such that

$$(\Pi_h^{\mathcal{RT},1} \underline{g}, \underline{w}_h)_{L^2(Q)} = (\underline{g}, \underline{w}_h)_{L^2(Q)} \quad (21)$$

for all $\underline{w}_h \in S^1(\mathcal{T}_\alpha^t) \otimes \mathcal{RT}^0(\mathcal{T}_\nu^x)$. Note that both $L^2(Q)$ projections possibly have inhomogeneous Dirichlet, initial or terminal conditions.

6 FEM for the vectorial wave equation

Following the introduction to the finite element spaces in the last section, we derive conforming space-time discretizations for the variational formulations (10), (17), using the notation of Section 5. For this purpose, let the bounded Lipschitz domain $\Omega \subset \mathbb{R}^d$ be polygonal for $d = 2$, or polyhedral for $d = 3$. Additionally, we assume Assumption 4.1 and the assumptions on the mesh stated in Section 5.

6.1 Galerkin–Petrov FEM

In this subsection, we state the conforming discretization of the variational formulation (10), using the tensor-product spaces (18), (19), by a Galerkin–Petrov finite element method:

Find $\underline{A}_h \in S_{0,0}^1(\mathcal{T}_\alpha^t) \otimes \mathcal{N}_{1,0}^0(\mathcal{T}_\nu^x)$ such that

$$-(\epsilon \partial_t \underline{A}_h, \partial_t \underline{w}_h)_{L^2(Q)} + (\mu^{-1} \operatorname{curl}_x \underline{A}_h, \operatorname{curl}_x \underline{w}_h)_{L^2(Q)} = (\Pi_h \underline{j}, \underline{w}_h)_{L^2(Q)} \quad (22)$$

for all $\underline{w}_h \in S_{0,0}^1(\mathcal{T}_\alpha^t) \otimes \mathcal{N}_{1,0}^0(\mathcal{T}_\nu^x)$. Hence, we approximate the solution $\underline{A} \in H_{0,0}^{\operatorname{curl};1}(Q)$ of the variational formulation (10) by

$$\underline{A}(t, x) \approx \underline{A}_h(t, x) = \sum_{k=1}^{N^t} \sum_{\kappa=1}^{N_x^N} \mathcal{A}_\kappa^k \varphi_\kappa^1(t) \psi_\kappa^N(x), \quad (t, x) \in Q, \quad (23)$$

with coefficients $\mathcal{A}_\kappa^k \in \mathbb{R}$. The operator Π_h in (22) is either the $L^2(Q)$ projection Π_h^0 onto the space of piecewise constant functions defined in (20) or the $L^2(Q)$ projection $\Pi_h^{\mathcal{RT},1}$ onto piecewise linear functions in time and Raviart–Thomas functions in space given in (21). The reason to replace the right-hand side \underline{j} with $\Pi_h \underline{j}$ in (22) is the comparison with the Galerkin–Bubnov finite element method (40), using the modified Hilbert transformation \mathcal{H}_T . An alternative is the use of formulas for numerical integration applied to $(\underline{j}, \underline{w}_h)_{L^2(Q)}$. Note that such formulas for numerical integration have to be sufficiently accurate to preserve the convergence rates of the finite element method, see the numerical examples in Section 7.

Next, we use the representation (23) to rewrite the discrete variational formulation (22) into the equivalent linear system

$$(-A_{ht}^1 \otimes M_{hx}^N + M_{ht}^1 \otimes A_{hx}^N) \underline{A} = \underline{\mathcal{J}}. \quad (24)$$

Here, we order the degrees of freedom first in time then in space so that the coefficient vector in (23) can be written as

$$\underline{A} = (\underline{\mathcal{A}}^1, \underline{\mathcal{A}}^2, \dots, \underline{\mathcal{A}}^{N^t})^\top \in \mathbb{R}^{N^t N_x^N}, \quad (25)$$

where

$$\underline{\mathcal{A}}^k = (\mathcal{A}_1^k, \mathcal{A}_2^k, \dots, \mathcal{A}_{N_x^{\mathcal{N}}}^k)^\top \in \mathbb{R}^{N_x^{\mathcal{N}}} \quad \text{for } k = 1, \dots, N^t.$$

Further, for the linear system (24), we define the spatial matrices by

$$A_{h_x}^{\mathcal{N}}[\ell, \kappa] = (\mu^{-1} \operatorname{curl}_x \underline{\psi}_\kappa^{\mathcal{N}}, \operatorname{curl}_x \underline{\psi}_\ell^{\mathcal{N}})_{L^2(\Omega)}, \quad M_{h_x}^{\mathcal{N}}[\ell, \kappa] = (\epsilon \underline{\psi}_\kappa^{\mathcal{N}}, \underline{\psi}_\ell^{\mathcal{N}})_{L^2(\Omega)} \quad (26)$$

for $\ell, \kappa = 1, \dots, N_x^{\mathcal{N}}$ and the temporal matrices by

$$A_{h_t}^1[l, k] = (\partial_t \varphi_k^1, \partial_t \varphi_l^1)_{L^2(0, T)}, \quad M_{h_t}^1[l, k] = (\varphi_k^1, \varphi_l^1)_{L^2(0, T)} \quad (27)$$

for $l = 0, \dots, N^t - 1, k = 1, \dots, N^t$ as well as the right-hand side by

$$\underline{\mathcal{J}} = (\underline{f}^0, \underline{f}^1, \dots, \underline{f}^{N^t-1})^\top \in \mathbb{R}^{N^t N_x^{\mathcal{N}}}$$

with $\underline{f}^l = (f_1^l, f_2^l, \dots, f_{N_x^{\mathcal{N}}}^l)^\top \in \mathbb{R}^{N_x^{\mathcal{N}}}$ for $l = 0, \dots, N^t - 1$ and

$$f_\ell^l = (\Pi_{h_j} j, \varphi_l^1 \underline{\psi}_\ell^{\mathcal{N}})_{L^2(Q)} \quad \text{for } l = 0, \dots, N^t - 1, \ell = 1, \dots, N_x^{\mathcal{N}}. \quad (28)$$

For the stability analysis of the linear system (24), we take a closer look at the system matrix. The system matrix of the linear system (24) is sparse and allows for a realization as a two-step method, due to the sparsity pattern of the temporal matrices $A_{h_t}^1, M_{h_t}^1$ in (27). Further, this sparsity pattern forms the basis of classical stability analysis of the Galerkin–Petrov finite element method (22) in the framework of time-stepping or finite difference methods. See [31, Section 5] for the scalar wave equation, where the ideas can be extended to the vectorial wave equation, see the discussion in [15, Section 3.5.2] or [17]. Here, we skip details and only state that the Galerkin–Petrov finite element method (22) is stable if the temporal mesh is uniform with mesh size h_t and the CFL condition

$$h_t < \sqrt{\frac{12}{c_1}} h_x \quad (29)$$

is satisfied with the constant $c_1 > 0$ of the spatial inverse inequality

$$\forall v_{h_x} \in \mathcal{N}_1^0(\mathcal{T}_\nu^x) : \quad \|\operatorname{curl}_x v_{h_x}\|_{L^2(\Omega)}^2 \leq c_1 h_x^{-2} \|v_{h_x}\|_{L^2(\Omega)}^2. \quad (30)$$

Bounds for the constant $c_1 > 0$ are given in [15, Lemma A.2] or [16, 17].

As an example domain, which is also used in Section 7, we consider the unit square $\Omega = (0, 1) \times (0, 1) \subset \mathbb{R}^2$. Using uniform triangulations with isosceles right triangles as in Figure 1 yields the constant $c_1 = 18$. This result is proven by adapting the arguments of the proof of (30), given in [15, Lemma A.2] or [17], of the general situation to the case of isosceles right triangles. More precisely, in the proof of [15, Lemma A.2], the matrix $J_l J_l^\top$ is diagonal for isosceles right triangles, where J_l denotes the Jacobian matrix of the geometric mapping from the reference element to the physical one. Thus, the eigenvalues of $J_l J_l^\top$ are known explicitly. So, in this situation, the CFL condition (29) reads as

$$h_t < \sqrt{\frac{12}{18}} h_x \approx 0.81649658 h_x. \quad (31)$$

Numerical examples indicate the sharpness of the CFL condition (31), see Subsection 7.1.

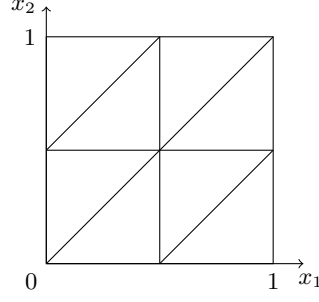


Figure 1: Uniform triangulations of the unit square with isosceles right triangles.

6.1.1 Using the $L^2(Q)$ projection $\Pi_h = \Pi_h^0$ for the right-hand side $\underline{\mathcal{J}}$

We present the calculation of the right-hand side $\underline{\mathcal{J}}$ of the linear system (24) when Π_h is the $L^2(Q)$ projection onto $S^0(\mathcal{T}_\alpha^t) \otimes S_d^0(\mathcal{T}_\nu^x)$ satisfying

$$(\Pi_h^0 \underline{j}, \underline{w}_h)_{L^2(Q)} = (\underline{j}, \underline{w}_h)_{L^2(Q)}$$

for all $\underline{w}_h \in S^0(\mathcal{T}_\alpha^t) \otimes S_d^0(\mathcal{T}_\nu^x)$. Then the projection $\Pi_h^0 \underline{j}$ is the solution of the linear system

$$M_{h_t}^0 \otimes M_{h_x}^0 (\underline{j}^1, \dots, \underline{j}^{N^t})^\top = (\hat{j}^1, \dots, \hat{j}^{N^t})^\top \quad (32)$$

with the matrices and vectors

$$\begin{aligned} M_{h_t}^0[l, k] &= (\varphi_k^0, \varphi_l^0)_{L^2(0, T)}, & l, k &= 1, \dots, N^t, \\ M_{h_x}^0[\ell, \kappa] &= (\underline{\psi}_\kappa^0, \underline{\psi}_\ell^0)_{L^2(\Omega)}, & \ell, \kappa &= 1, \dots, N_x^0, \\ \underline{j}^k[\kappa] &= j_\kappa^k, & k &= 1, \dots, N^t, \kappa = 1, \dots, N_x^0, \\ \hat{j}^k[\kappa] &= (\underline{j}, \varphi_k^0 \underline{\psi}_\kappa^0)_{L^2(Q)}, & k &= 1, \dots, N^t, \kappa = 1, \dots, N_x^0, \end{aligned}$$

through the representation

$$\Pi_h^0 \underline{j}(t, x) = \sum_{k=1}^{N^t} \sum_{\kappa=1}^{N_x^0} j_\kappa^k \varphi_k^0(t) \underline{\psi}_\kappa^0(x), \quad (t, x) \in Q.$$

Thus, using this representation for the right-hand side (28) of the space-time Galerkin–Petrov method (24) yields

$$f_\ell^l = (\Pi_h^0 \underline{j}, \varphi_l^1 \underline{\psi}_\ell^N)_{L^2(Q)} = \sum_{k=1}^{N^t} \sum_{\kappa=1}^{N_x^0} j_\kappa^k \underbrace{(\varphi_k^0, \varphi_l^1)_{L^2(0, T)}}_{=M_{h_t}^{1,0}[l, k]} \underbrace{(\underline{\psi}_\kappa^0, \underline{\psi}_\ell^N)_{L^2(\Omega)}}_{=M_{h_x}^{N,0}[\ell, \kappa]} = F[l, \ell]$$

for $\ell = 1, \dots, N_x^N$, $l = 0, \dots, N^t - 1$ with the matrix

$$F = M_{h_x}^{N,0} J (M_{h_t}^{1,0})^\top \in \mathbb{R}^{N_x^N \times N^t},$$

where

$$M_{h_x}^{N,0}[\ell, \kappa] = (\underline{\psi}_\kappa^0, \underline{\psi}_\ell^N)_{L^2(\Omega)} \quad \ell = 1, \dots, N_x^N, \quad \kappa = 1, \dots, N_x^0, \quad (33)$$

$$J[\kappa, k] = j_\kappa^k, \quad \kappa = 1, \dots, N_x^0, \quad k = 1, \dots, N^t, \quad (34)$$

$$M_{h_t}^{1,0}[l, k] = (\varphi_k^0, \varphi_l^1)_{L^2(0,T)}, \quad l = 0, \dots, N^t - 1, \quad k = 1, \dots, N^t.$$

6.1.2 Using the $L^2(Q)$ projection $\Pi_h = \Pi_h^{\mathcal{RT},1}$ for the right-hand side $\underline{\mathcal{J}}$

Analogously to Subsection 6.1.1, we present the calculation of the right-hand side $\underline{\mathcal{J}}$ of the linear system (24) when Π_h is the $L^2(Q)$ projection onto $S^1(\mathcal{T}_\alpha^t) \otimes \mathcal{RT}^0(\mathcal{T}_\nu^x)$ given in (21). The projection $\Pi_h^{\mathcal{RT},1} \underline{j}$ is the solution of the linear system

$$\widetilde{M}_{h_t}^1 \otimes M_{h_x}^{\mathcal{RT}} (\underline{j}^0, \underline{j}^1, \dots, \underline{j}^{N^t})^\top = (\hat{\underline{j}}^0, \hat{\underline{j}}^1, \dots, \hat{\underline{j}}^{N^t})^\top \quad (35)$$

with the matrices and vectors

$$\begin{aligned} \widetilde{M}_{h_t}^1[l, k] &= (\varphi_k^1, \varphi_l^1)_{L^2(0,T)}, & l, k &= 0, \dots, N^t, & (36) \\ M_{h_x}^{\mathcal{RT}}[\ell, \kappa] &= (\underline{\psi}_\kappa^{\mathcal{RT}}, \underline{\psi}_\ell^{\mathcal{RT}})_{L^2(\Omega)}, & \ell, \kappa &= 1, \dots, N_x^{\mathcal{RT}}, \\ \underline{j}^k[\kappa] &= j_\kappa^k, & k &= 0, \dots, N^t, \quad \kappa = 1, \dots, N_x^{\mathcal{RT}}, \\ \hat{\underline{j}}^k[\kappa] &= (\underline{j}, \varphi_k^1 \underline{\psi}_\kappa^{\mathcal{RT}})_{L^2(Q)}, & k &= 0, \dots, N^t, \quad \kappa = 1, \dots, N_x^{\mathcal{RT}}, \end{aligned}$$

by the representation

$$\Pi_h^{\mathcal{RT},1} \underline{j}(t, x) = \sum_{k=0}^{N^t} \sum_{\kappa=1}^{N_x^{\mathcal{RT}}} j_\kappa^k \varphi_k^1(t) \underline{\psi}_\kappa^{\mathcal{RT}}(x), \quad (t, x) \in Q.$$

Thus, using this representation for the right-hand side (28) yields

$$f_\ell^l = (\Pi_h^{\mathcal{RT},1} \underline{j}, \varphi_l^1 \underline{\psi}_\ell^N)_{L^2(Q)} = \sum_{k=0}^{N^t} \sum_{\kappa=1}^{N_x^{\mathcal{RT}}} j_\kappa^k \underbrace{(\varphi_k^1, \varphi_l^1)_{L^2(0,T)}}_{=\widehat{M}_{h_t}^1[l,k]} \underbrace{(\underline{\psi}_\kappa^{\mathcal{RT}}, \underline{\psi}_\ell^N)_{L^2(\Omega)}}_{=M_{h_x}^{N,\mathcal{RT}}[\ell,\kappa]} = F[\ell, l]$$

for $\ell = 1, \dots, N_x^N$, $l = 0, \dots, N^t - 1$ with the matrix

$$F = M_{h_x}^{N,\mathcal{RT}} J(\widehat{M}_{h_t}^1)^\top \in \mathbb{R}^{N_x^N \times N^t},$$

where

$$M_{h_x}^{N,\mathcal{RT}}[\ell, \kappa] = (\underline{\psi}_\kappa^{\mathcal{RT}}, \underline{\psi}_\ell^N)_{L^2(\Omega)}, \quad \ell = 1, \dots, N_x^N, \quad \kappa = 1, \dots, N_x^{\mathcal{RT}}, \quad (37)$$

$$J[\kappa, k] = j_\kappa^k, \quad \kappa = 1, \dots, N_x^{\mathcal{RT}}, \quad k = 0, \dots, N^t, \quad (38)$$

$$\widehat{M}_{h_t}^1[l, k] = (\varphi_k^1, \varphi_l^1)_{L^2(0,T)}, \quad l = 0, \dots, N^t - 1, \quad k = 0, \dots, N^t. \quad (39)$$

Note that the matrices $M_{h_t}^1 \in \mathbb{R}^{N^t \times N^t}$ in (27) and $\widehat{M}_{h_t}^1 \in \mathbb{R}^{N^t \times (N^t+1)}$ in (39) are submatrices of the matrix $\widetilde{M}_{h_t}^1 \in \mathbb{R}^{(N^t+1) \times (N^t+1)}$ in (36).

6.2 Galerkin–Bubnov FEM

In this subsection, we discretize the variational formulation (17) where we apply the modified Hilbert transformation. We use a tensor-product ansatz and the conforming finite element space (18). In particular, we consider the Galerkin–Bubnov finite element method to find $\underline{A}_h \in S_{0,\alpha}^1(\mathcal{T}_\alpha^t) \otimes \mathcal{N}_{1,0}^0(\mathcal{T}_\nu^x)$ such that

$$(\epsilon \mathcal{H}_T \partial_t \underline{A}_h, \partial_t \underline{v}_h)_{L^2(Q)} + (\mu^{-1} \operatorname{curl}_x \underline{A}_h, \operatorname{curl}_x \mathcal{H}_T \underline{v}_h)_{L^2(Q)} = (\Pi_h \underline{j}, \mathcal{H}_T \underline{v}_h)_{L^2(Q)} \quad (40)$$

for all $\underline{v}_h \in S_{0,\alpha}^1(\mathcal{T}_\alpha^t) \otimes \mathcal{N}_{1,0}^0(\mathcal{T}_\nu^x)$. Again, Π_h is either the $L^2(Q)$ projection Π_h^0 defined in (20) or the $L^2(Q)$ projection $\Pi_h^{\mathcal{RT},1}$ given in (21).

The discrete variational formulation (40) is equivalent to the linear system

$$(A_{h_t}^{\mathcal{H}_T} \otimes M_{h_x}^{\mathcal{N}} + M_{h_t}^{\mathcal{H}_T} \otimes A_{h_x}^{\mathcal{N}}) \underline{A} = \underline{\mathcal{J}}^{\mathcal{H}_T} \quad (41)$$

with the spatial matrices $A_{h_x}^{\mathcal{N}}, M_{h_x}^{\mathcal{N}}$ given in (26) and the temporal matrices

$$A_{h_t}^{\mathcal{H}_T}[l, k] = (\mathcal{H}_T \partial_t \varphi_k^1, \partial_t \varphi_l^1)_{L^2(0,T)}, \quad M_{h_t}^{\mathcal{H}_T}[l, k] = (\varphi_k^1, \mathcal{H}_T \varphi_l^1)_{L^2(0,T)} \quad (42)$$

for $l, k = 1, \dots, N^t$, where \mathcal{H}_T , defined in Section 3, acts solely on time-dependent functions. As in Subsection 6.1, we use again the representation (23) of \underline{A}_h and the vector $\underline{A} \in \mathbb{R}^{N^t N_x^{\mathcal{N}}}$ of its coefficients (25). The right-hand side of the linear system (41) is given by

$$\underline{\mathcal{J}}^{\mathcal{H}_T} = (\underline{\mathcal{J}}^1, \underline{\mathcal{J}}^2, \dots, \underline{\mathcal{J}}^{N^t})^\top \in \mathbb{R}^{N^t N_x^{\mathcal{N}}}$$

with

$$\underline{\mathcal{J}}^l = (\mathcal{J}_1^l, \mathcal{J}_2^l, \dots, \mathcal{J}_{N_x^{\mathcal{N}}}^l)^\top \in \mathbb{R}^{N_x^{\mathcal{N}}} \quad \text{for } l = 1, \dots, N^t,$$

where

$$\mathcal{J}_\ell^l = (\Pi_h \underline{j}, \psi_\ell^{\mathcal{N}} \mathcal{H}_T \varphi_l^1)_{L^2(Q)} \quad \text{for } l = 1, \dots, N^t, \ell = 1, \dots, N_x^{\mathcal{N}}. \quad (43)$$

Let us take a look at the solvability of the system matrix of the linear system (41). The temporal matrices $A_{h_t}^{\mathcal{H}_T}, M_{h_t}^{\mathcal{H}_T}$ in (42) are positive definite due to property (6). In addition, the spatial matrix $M_{h_x}^{\mathcal{N}}$ in (26) is also positive definite, whereas the spatial matrix $A_{h_x}^{\mathcal{N}}$ in (26) is only positive semi-definite. Hence, the Kronecker product $A_{h_t}^{\mathcal{H}_T} \otimes M_{h_x}^{\mathcal{N}}$ is positive definite. On the other hand, the product $M_{h_t}^{\mathcal{H}_T} \otimes A_{h_x}^{\mathcal{N}}$ is positive semi-definite. Adding both results in a positive definite system matrix of the linear system (41). In other words, the linear system (41) is uniquely solvable. Note that, compared to the static case, we do not need any stabilization to get unique solvability of the linear system (41) and hence of the corresponding discrete variational formulation (40). However, further details on the numerical analysis of the Galerkin–Bubnov finite element method (40) are far beyond the scope of this contribution, we refer to [26, 27] for the case of the scalar wave equation.

In addition, note that the temporal matrices $A_{h_t}^{\mathcal{H}_T}, M_{h_t}^{\mathcal{H}_T}$ in (42) are dense, whereas the spatial matrices $A_{h_x}^{\mathcal{N}}, M_{h_x}^{\mathcal{N}}$ in (26) are sparse. Thus, the linear system (41) does not allow for a realization as a multistep method. However, the application of fast (direct) solvers, as known for heat and scalar wave equations [23, 37, 38], is possible, which is the topic of future work.

6.2.1 Using the $L^2(Q)$ projection $\Pi_h = \Pi_h^0$ for the right-hand side $\underline{\mathcal{J}}^{\mathcal{H}T}$

In this subsection, we present the calculation of the right-hand side $\underline{\mathcal{J}}^{\mathcal{H}T}$ of the linear system (41) when Π_h is the $L^2(Q)$ projection onto $S^0(\mathcal{T}_\alpha^t) \otimes S_d^0(\mathcal{T}_\nu^x)$ given in (20). Since this subsection is similar to Subsection 6.1.1, we skip the details.

Then the entries (43) of the right-hand side $\underline{\mathcal{J}}^{\mathcal{H}T}$ admit the representation

$$\mathcal{J}_\ell^l = (\Pi_h^0 \underline{j}, \underline{\psi}_\ell^N \mathcal{H}_T \varphi_l^1)_{L^2(Q)} = F^{\mathcal{H}T}[\ell, l]$$

for $\ell = 1, \dots, N_x^N$, $l = 1, \dots, N^t$ with the matrix

$$F^{\mathcal{H}T} = M_{h_x}^{N,0} J(M_{h_t}^{\mathcal{H}T,1,0})^\top \in \mathbb{R}^{N_x^N \times N^t},$$

where $M_{h_x}^{N,0}$ is defined in (33), J is given in (34) and

$$M_{h_t}^{\mathcal{H}T,1,0}[l, k] = (\varphi_k^0, \mathcal{H}_T \varphi_l^1)_{L^2(0,T)}, \quad l = 1, \dots, N^t, \quad k = 1, \dots, N^t.$$

6.2.2 Using the $L^2(Q)$ projection $\Pi_h = \Pi_h^{\mathcal{RT},1}$ for the right-hand side $\underline{\mathcal{J}}^{\mathcal{H}T}$

Analogously to Subsection 6.2.1, we present the calculation of the right-hand side $\underline{\mathcal{J}}^{\mathcal{H}T}$ of the linear system (41) when Π_h is the $L^2(Q)$ projection onto $S^1(\mathcal{T}_\alpha^t) \otimes \mathcal{RT}^0(\mathcal{T}_\nu^x)$ given in (21). As for Subsection 6.2.1, we skip the details, which are analogous to Subsection 6.1.2.

Then the entries (43) of the right-hand side $\underline{\mathcal{J}}^{\mathcal{H}T}$ admit the representation

$$\mathcal{J}_\ell^l = (\Pi_h^{\mathcal{RT},1} \underline{j}, \underline{\psi}_\ell^N \mathcal{H}_T \varphi_l^1)_{L^2(Q)} = F^{\mathcal{H}T}[\ell, l]$$

for $\ell = 1, \dots, N_x^N$, $l = 1, \dots, N^t$ with the matrix

$$F^{\mathcal{H}T} = M_{h_x}^{N,\mathcal{RT}} J(\widehat{M}_{h_t}^{\mathcal{H}T})^\top \in \mathbb{R}^{N_x^N \times N^t},$$

where $M_{h_x}^{N,\mathcal{RT}}$ is defined in (37), J is given in (38) and

$$\widehat{M}_{h_t}^{\mathcal{H}T}[l, k] = (\varphi_k^1, \mathcal{H}_T \varphi_l^1)_{L^2(0,T)}, \quad l = 1, \dots, N^t, \quad k = 0, \dots, N^t. \quad (44)$$

Note that the matrix $M_{h_t}^{\mathcal{H}T} \in \mathbb{R}^{N^t \times N^t}$ in (42) is a submatrix of $\widehat{M}_{h_t}^{\mathcal{H}T} \in \mathbb{R}^{N^t \times (N^t+1)}$ in (44).

7 Numerical examples for the vectorial wave equation

In this section, we give numerical examples of the conforming space-time finite element methods (22) and (40) for a spatially two-dimensional domain $\Omega \subset \mathbb{R}^2$, i.e. $d = 2$. For this purpose, we consider the unit square $\Omega = (0, 1) \times (0, 1)$, and set $\epsilon(x) = \begin{pmatrix} 1 & 0 \\ 0 & 1 \end{pmatrix}$, $\mu(x) = 1$ for $x \in \Omega$. The spatial meshes \mathcal{T}_ν^x are given by uniform decompositions of the spatial domain Ω into isosceles right triangles, where a uniform refinement strategy is applied, see Figure 2. We investigate the terminal times $T \in \{\sqrt{2}, \frac{3}{2}\}$ to examine the CFL condition (31) of the Galerkin–Petrov finite element method (22). The temporal meshes \mathcal{T}_α^t are defined by $t_l = \frac{Tl}{N_\alpha^t}$ for $l = 0, \dots, N_\alpha^t$, where $N_\alpha^t = 5 \cdot 2^\alpha$, $\alpha = 0, \dots, 4$. Note that for this choice of spatial and temporal meshes, we are in the framework of the CFL condition (31).

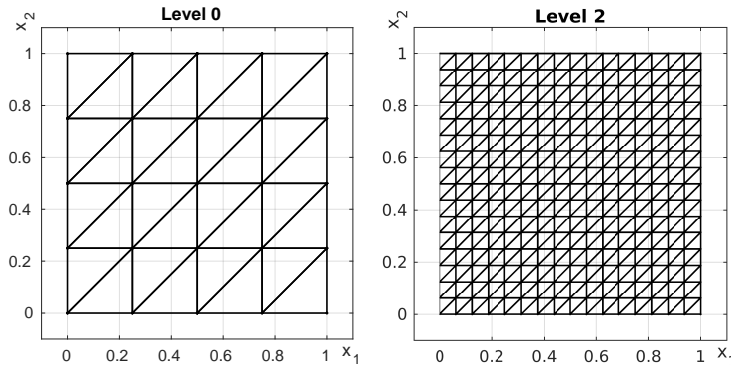


Figure 2: Spatial meshes \mathcal{T}_ν^x : Initial mesh \mathcal{T}_0^x and the mesh \mathcal{T}_2^x after two uniform refinements.

In the following numerical examples, we measure the error of the space-time finite element methods (22) and (40) in the space-time norms $\|\cdot\|_{L^2(Q)}$ and $|\cdot|_{H^{\text{curl};1}(Q)}$. In particular, we state the numerical results for $\|\underline{A} - \underline{A}_h\|_{L^2(Q)}$ and

$$|\underline{A} - \underline{A}_h|_{H^{\text{curl};1}(Q)} = \left(\|\partial_t \underline{A} - \partial_t \underline{A}_h\|_{L^2(Q)}^2 + \|\text{curl}_x \underline{A} - \text{curl}_x \underline{A}_h\|_{L^2(Q)}^2 \right)^{1/2},$$

where $\underline{A} \in H_{0;0}^{\text{curl};1}(Q)$ is the solution of the variational formulation (10), and $\underline{A}_h \in S_0^1(\mathcal{T}_\alpha^t) \otimes \mathcal{N}_{1,0}^0(\mathcal{T}_\nu^x)$ is the solution of space-time finite element method (22) or (40). For the vectorial wave equation (3) and its variational formulation (10), we use the manufactured solution

$$\underline{A}(t, x_1, x_2) = \begin{pmatrix} A_1(t, x_1, x_2) \\ A_2(t, x_1, x_2) \end{pmatrix} = \begin{pmatrix} -5t^2 x_2(1 - x_2) \\ t^2 x_1(1 - x_1) \end{pmatrix} + t^3 \begin{pmatrix} \sin(\pi x_1) x_2(1 - x_2) \\ 0 \end{pmatrix} \quad (45)$$

for $(t, x_1, x_2) \in \bar{Q}$, which is, for comparison, also investigated in [16]. This solution satisfies the homogeneous Dirichlet condition $\gamma_t \underline{A}(t, x_1, x_2) = \underline{A}|_\Sigma(t, x_1, x_2) \times \underline{n}_x(x_1, x_2) = 0$ for $(t, x_1, x_2) \in \Sigma$ as well as the homogeneous initial conditions $\underline{A}(0, x_1, x_2) = \partial_t \underline{A}(0, x_1, x_2) = 0$ for $(x_1, x_2) \in \Omega$. The related right-hand side \underline{j} is given by

$$\underline{j}(t, x_1, x_2) = \begin{pmatrix} -10(t^2 - x_2^2 + x_2) \\ 2(t^2 - x_1^2 + x_1) \end{pmatrix} + \begin{pmatrix} 2t^3 \sin(\pi x_1) + 6t \sin(\pi x_1) x_2(1 - x_2) \\ \pi t^3(1 - 2x_2) \cos(\pi x_1) \end{pmatrix}, \quad (t, x_1, x_2) \in Q.$$

For the computations, we use high-order quadrature rules to calculate the integrals for computing the projections $\Pi_h^0 \underline{j}$, $\Pi_h^{\mathcal{RT},1} \underline{j}$ in (32), (35). The temporal matrices involving the modified Hilbert transformation \mathcal{H}_T , e.g. the matrices (42), are assembled as proposed in [40, Subsection 2.2], see also [41] for further assembling strategies. All spatial matrices, e.g. the matrices (26), are calculated with the help of the finite element library Netgen/NGSolve, see www.ngsolve.org and [29]. We solve the linear systems using the sparse direct solver UMFPACK 5.7.1 [9] in the standard configuration. All calculations, presented in this section, were performed on a PC with two Intel Xeon E5-2687W v4 CPUs 3.00 GHz, i.e. in sum 24 cores and 512 GB main memory.

Last, in Table 1, Table 2, we report the interpolation error in the norms $|\cdot|_{H^{\text{curl};1}(Q)}$ and $\|\cdot\|_{L^2(Q)}$ for the unit square Ω and $T = \sqrt{2}$ for the function \underline{A} defined in (45), where first-order convergence is observed in $|\cdot|_{H^{\text{curl};1}(Q)}$ and second-order convergence is obtained in $\|\cdot\|_{L^2(Q)}$.

$h_x \backslash h_t$	0.2828	0.1414	0.0707	0.0354	0.0177
0.1768	6.64e-01	6.53e-01	6.50e-01	6.49e-01	6.49e-01
0.0884	3.49e-01	3.27e-01	3.21e-01	3.20e-01	3.20e-01
0.0442	2.12e-01	1.74e-01	1.63e-01	1.60e-01	1.59e-01
0.0221	1.61e-01	1.06e-01	8.68e-02	8.13e-02	7.99e-02
0.0110	1.46e-01	8.04e-02	5.29e-02	4.34e-02	4.07e-02

Table 1: Interpolation errors in $|\cdot|_{H^{\text{curl};1}(Q)}$ for $T = \sqrt{2}$, the unit square Ω and \underline{A} in (45).

$h_x \backslash h_t$	0.2828	0.1414	0.0707	0.0354	0.0177
0.1768	7.50e-02	7.49e-02	7.49e-02	7.49e-02	7.49e-02
0.0884	1.99e-02	1.93e-02	1.93e-02	1.93e-02	1.93e-02
0.0442	6.97e-03	4.96e-03	4.82e-03	4.81e-03	4.81e-03
0.0221	5.25e-03	1.74e-03	1.24e-03	1.20e-03	1.20e-03
0.0110	5.13e-03	1.31e-03	4.37e-04	3.11e-04	3.01e-04

Table 2: Interpolation errors in $\|\cdot\|_{L^2(Q)}$ for $T = \sqrt{2}$, the unit square Ω and \underline{A} in (45).

7.1 Galerkin–Petrov FEM

In this subsection, we investigate numerical examples for the Galerkin–Petrov finite element method (22) in the situation described at the beginning of this section.

$h_x \backslash h_t$	0.2828	0.1414	0.0707	0.0354	0.0177
0.1768	6.68e-01	6.55e-01	6.52e-01	6.52e-01	6.51e-01
0.0884	3.56e-01	9.03e-01	3.27e-01	3.26e-01	3.26e-01
0.0442	2.18e-01	7.22e-01	4.37e+03	1.64e-01	1.63e-01
0.0221	1.66e-01	2.19e-01	2.02e+04	8.75e+13	8.19e-02
0.0110	1.50e-01	9.82e-02	8.64e+03	5.02e+17	8.43e+21

Table 3: Errors in $|\cdot|_{H^{\text{curl};1}(Q)}$ of the Galerkin–Petrov FEM (22) with the approximate right-hand side $\Pi_{h\underline{j}}^0 \in S^0(\mathcal{T}_\alpha^t) \otimes S_2^0(\mathcal{T}_\nu^x)$ for $T = \sqrt{2}$, the unit square Ω and \underline{A} in (45).

$h_x \backslash h_t$	0.2828	0.1414	0.0707	0.0354	0.0177
0.1768	9.79e-02	9.73e-02	9.73e-02	9.73e-02	9.73e-02
0.0884	4.83e-02	4.95e-02	4.67e-02	4.67e-02	4.67e-02
0.0442	2.64e-02	2.47e-02	4.27e+01	2.33e-02	2.33e-02
0.0221	1.70e-02	1.22e-02	1.09e+02	4.55e+11	1.17e-02
0.0110	1.37e-02	6.63e-03	2.69e+01	1.56e+15	2.28e+19

Table 4: Errors in $\|\cdot\|_{L^2(Q)}$ of the Galerkin–Petrov FEM (22) with the approximate right-hand side $\Pi_{h\underline{j}}^0 \in S^0(\mathcal{T}_\alpha^t) \otimes S_2^0(\mathcal{T}_\nu^x)$ for $T = \sqrt{2}$, the unit square Ω and \underline{A} in (45).

First, we consider the terminal time $T = \sqrt{2}$. In Table 3 and Table 4, we present the numerical results for the Galerkin–Petrov finite element method (22) with the approximate

$h_x \backslash h_t$	0.2828	0.1414	0.0707	0.0354	0.0177
0.1768	6.38e-01	6.26e-01	6.23e-01	6.22e-01	6.22e-01
0.0884	3.42e-01	8.26e-01	3.10e-01	3.09e-01	3.08e-01
0.0442	2.16e-01	9.97e-01	3.70e+03	1.55e-01	1.54e-01
0.0221	1.72e-01	1.06e+00	1.81e+04	6.10e+13	7.73e-02
0.0110	1.59e-01	1.24e+00	1.91e+04	5.71e+18	3.25e+21

Table 5: Errors in $|\cdot|_{H^{\text{curl};1}(Q)}$ of the Galerkin–Petrov FEM (22) with the approximate right-hand side $\Pi_h^{\mathcal{RT},1} \underline{j} \in S^1(\mathcal{T}_\alpha^t) \otimes \mathcal{RT}^0(\mathcal{T}_\nu^x)$ for $T = \sqrt{2}$, the unit square Ω and \underline{A} in (45).

$h_x \backslash h_t$	0.2828	0.1414	0.0707	0.0354	0.0177
0.1768	4.67e-02	4.29e-02	4.21e-02	4.19e-02	4.19e-02
0.0884	1.80e-02	1.93e-02	1.06e-02	1.04e-02	1.04e-02
0.0442	1.27e-02	1.32e-02	3.61e+01	2.66e-03	2.61e-03
0.0221	1.18e-02	1.36e-02	1.01e+02	3.17e+11	6.64e-04
0.0110	1.16e-02	1.53e-02	8.53e+01	1.74e+16	8.78e+18

Table 6: Errors in $\|\cdot\|_{L^2(Q)}$ of the Galerkin–Petrov FEM (22) with the approximate right-hand side $\Pi_h^{\mathcal{RT},1} \underline{j} \in S^1(\mathcal{T}_\alpha^t) \otimes \mathcal{RT}^0(\mathcal{T}_\nu^x)$ for $T = \sqrt{2}$, the unit square Ω and \underline{A} in (45).

right-hand side $\Pi_h^0 \underline{j} \in S^0(\mathcal{T}_\alpha^t) \otimes S_2^0(\mathcal{T}_\nu^x)$ of Subsection 6.1.1. In Table 5 and Table 6, we report the results for $\Pi_h^{\mathcal{RT},1} \underline{j} \in S^1(\mathcal{T}_\alpha^t) \otimes \mathcal{RT}^0(\mathcal{T}_\nu^x)$ of Subsection 6.1.2. All tables show conditional stability, i.e. the CFL condition (31) is required for stability. Note that the ratio of the mesh sizes $h_t = 0.0177$ and $h_x = 0.0221$, i.e. the last column and second last row of Tables 3 to 6, is given by

$$\frac{h_t}{h_x} \approx \frac{0.0177}{0.0221} \approx 0.801$$

and thus, fulfills the CFL condition (31) resulting in a stable method. In the case of stability, we observe first-order convergence in $|\cdot|_{H^{\text{curl};1}(Q)}$, where the errors in Table 1, Table 3 and Table 5 are within the same range. When considering the errors in $\|\cdot\|_{L^2(Q)}$, Table 4 reports only first-order convergence, whereas in Table 6, second-order convergence is observed as in Table 2 on the interpolation error.

Next, we elaborate on this convergence behavior by investigating the difference $|\underline{A}(T, x) - \underline{A}_h(T, x)|$ for $x \in \Omega$. For the mesh sizes $h_t = 0.0707$, $h_x = 0.0884$, we plot the function $\Omega \ni x \mapsto |\underline{A}(T, x) - \underline{A}_h(T, x)|$ in Figure 3 for both projections Π_h^0 and $\Pi_h^{\mathcal{RT},1}$. In the literature, we find the term *spurious solutions*, e.g. in [21], or *spurious modes*, e.g. in [5]. Spurious modes are parts of the numerical solution, which correspond to eigensolutions of the discrete differential operator. They are oscillations that should not be part of the computed solution. Spurious modes can be understood as numerically generated noise and have no physical meaning. An example can be found in [21, Figure 5.8]. In Figure 3, we obtain a similar noise behavior that occurs for the projection $\Pi_h^0 \underline{j}$ of the right-hand side. Here, we observe some of the zero eigensolutions of the curl-curl operator added to the solution. Hence, we get a worse $L^2(Q)$ -error, see Table 4 and Table 6, but a similar error behavior in the $|\cdot|_{H^{\text{curl};1}(Q)}$ -norm for both projections if the CFL condition is met, see Table 3 and Table 5.

To summarize, the approximation $\Pi_h^0 \underline{j} \in S^0(\mathcal{T}_\alpha^t) \otimes S_2^0(\mathcal{T}_\nu^x)$ of \underline{j} is good enough, when the

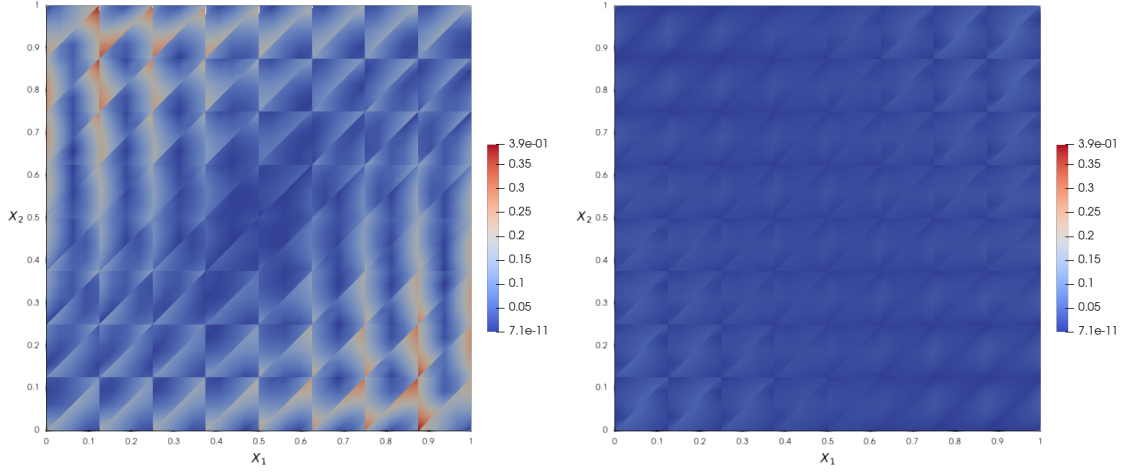


Figure 3: The magnitude of the difference $|\underline{A}(T, \cdot) - \underline{A}_h(T, \cdot)|$ for $T = \sqrt{2}$, $\nu = 1$, $\alpha = 2$, displayed over Ω for $\Pi_h^0 \underline{j} \in S^0(\mathcal{T}_\alpha^t) \otimes S_2^0(\mathcal{T}_\nu^x)$ (left) and $\Pi_h^{\mathcal{RT},1} \underline{j} \in S^1(\mathcal{T}_\alpha^t) \otimes \mathcal{RT}^0(\mathcal{T}_\nu^x)$ (right).

error is measured in $|\cdot|_{H^{\text{curl};1}(Q)}$, while the better approximation $\Pi_h^{\mathcal{RT},1} \underline{j} \in S^1(\mathcal{T}_\alpha^t) \otimes \mathcal{RT}^0(\mathcal{T}_\nu^x)$ of \underline{j} is needed for optimal convergence rates in $\|\cdot\|_{L^2(Q)}$.

Second, we examine the terminal time $T = \frac{3}{2}$. In Table 7, Table 8, the numerical results for the Galerkin–Petrov finite element method (22) with the approximate right-hand side $\Pi_h^{\mathcal{RT},1} \underline{j} \in S^1(\mathcal{T}_\alpha^t) \otimes \mathcal{RT}^0(\mathcal{T}_\nu^x)$ of Subsection 6.1.2 show that slightly violating the CFL condition (31) leads to instability. More precisely, the ratio of the mesh sizes $h_t = 0.0188$ and $h_x = 0.0221$, i.e. the last column and second last row of Table 7, Table 8, is given by

$$\frac{h_t}{h_x} \approx \frac{0.0188}{0.0221} \approx 0.851$$

and thus, violates the CFL condition (31) resulting in an unstable method. In other words, the CFL condition (31) seems to be sharp for this particular situation.

$h_x \backslash h_t$	0.3000	0.1500	0.0750	0.0375	0.0188
0.1768	7.31e-01	7.18e-01	7.16e-01	7.15e-01	7.15e-01
0.0884	3.90e-01	1.09e+00	3.57e-01	3.55e-01	3.55e-01
0.0442	2.44e-01	1.24e+00	6.37e+03	4.40e-01	1.77e-01
0.0221	1.92e-01	1.37e+00	2.28e+04	9.80e+14	1.29e+04
0.0110	1.77e-01	1.58e+00	2.44e+04	5.36e+17	7.84e+21

Table 7: Errors in $|\cdot|_{H^{\text{curl};1}(Q)}$ of the Galerkin–Petrov FEM (22) with the approximate right-hand side $\Pi_h^{\mathcal{RT},1} \underline{j} \in S^1(\mathcal{T}_\alpha^t) \otimes \mathcal{RT}^0(\mathcal{T}_\nu^x)$ for $T = \frac{3}{2}$, the unit square Ω and \underline{A} in (45).

7.2 Galerkin–Bubnov FEM

In this subsection, we report on numerical results for the Galerkin–Bubnov finite element method (40) using the modified Hilbert transformation in the situation described at the be-

$h_x \backslash h_t$	0.3000	0.1500	0.0750	0.0375	0.0188
0.1768	5.45e-02	5.06e-02	4.99e-02	4.97e-02	4.97e-02
0.0884	2.05e-02	2.49e-02	1.26e-02	1.24e-02	1.23e-02
0.0442	1.43e-02	1.69e-02	6.28e+01	4.40e-03	3.09e-03
0.0221	1.33e-02	1.85e-02	1.30e+02	5.17e+12	4.92e+01
0.0110	1.31e-02	2.05e-02	1.16e+02	1.67e+15	2.16e+19

Table 8: Errors in $\|\cdot\|_{L^2(Q)}$ of the Galerkin–Petrov FEM (22) with the approximate right-hand side $\Pi_h^{\mathcal{RT},1} \underline{j} \in S^1(\mathcal{T}_\alpha^t) \otimes \mathcal{RT}^0(\mathcal{T}_\nu^x)$ for $T = \frac{3}{2}$, the unit square Ω and \underline{A} in (45).

ginning of this section. We only show numerical results for the terminal time $T = \sqrt{2}$, as those for $T = \frac{3}{2}$ are similar.

$h_x \backslash h_t$	0.2828	0.1414	0.0707	0.0354	0.0177
0.1768	6.77e-01	6.58e-01	6.53e-01	6.52e-01	6.51e-01
0.0884	3.72e-01	3.36e-01	3.28e-01	3.26e-01	3.26e-01
0.0442	2.41e-01	1.83e-01	1.68e-01	1.64e-01	1.63e-01
0.0221	1.95e-01	1.16e-01	9.13e-02	8.40e-02	8.21e-02
0.0110	1.81e-01	9.25e-02	5.79e-02	4.56e-02	4.20e-02

Table 9: Errors in $|\cdot|_{H^{\text{curl};1}(Q)}$ of the Galerkin–Bubnov FEM (40) with the approximate right-hand side $\Pi_h^0 \underline{j} \in S^0(\mathcal{T}_\alpha^t) \otimes S_2^0(\mathcal{T}_\nu^x)$ for $T = \sqrt{2}$, the unit square Ω and \underline{A} in (45).

$h_x \backslash h_t$	0.2828	0.1414	0.0707	0.0354	0.0177
0.1768	1.03e-01	9.61e-02	9.70e-02	9.73e-02	9.73e-02
0.0884	5.20e-02	4.61e-02	4.65e-02	4.67e-02	4.67e-02
0.0442	2.98e-02	2.33e-02	2.32e-02	2.32e-02	2.33e-02
0.0221	2.08e-02	1.22e-02	1.16e-02	1.16e-02	1.16e-02
0.0110	1.79e-02	7.12e-03	5.91e-03	5.84e-03	5.83e-03

Table 10: Errors in $\|\cdot\|_{L^2(Q)}$ of the Galerkin–Bubnov FEM (40) with the approximate right-hand side $\Pi_h^0 \underline{j} \in S^0(\mathcal{T}_\alpha^t) \otimes S_2^0(\mathcal{T}_\nu^x)$ for $T = \sqrt{2}$, the unit square Ω and \underline{A} in (45).

$h_x \backslash h_t$	0.2828	0.1414	0.0707	0.0354	0.0177
0.1768	6.45e-01	6.27e-01	6.23e-01	6.23e-01	6.22e-01
0.0884	3.62e-01	3.19e-01	3.11e-01	3.09e-01	3.08e-01
0.0442	2.48e-01	1.75e-01	1.59e-01	1.55e-01	1.54e-01
0.0221	2.10e-01	1.13e-01	8.72e-02	7.95e-02	7.75e-02
0.0110	2.00e-01	9.14e-02	5.63e-02	4.36e-02	3.98e-02

Table 11: Errors in $|\cdot|_{H^{\text{curl};1}(Q)}$ of the Galerkin–Bubnov FEM (40) with the approximate right-hand side $\Pi_h^{\mathcal{RT},1} \underline{j} \in S^1(\mathcal{T}_\alpha^t) \otimes \mathcal{RT}^0(\mathcal{T}_\nu^x)$ for $T = \sqrt{2}$, the unit square Ω and \underline{A} in (45).

$h_x \backslash h_t$	0.2828	0.1414	0.0707	0.0354	0.0177
0.1768	5.28e-02	4.23e-02	4.20e-02	4.19e-02	4.19e-02
0.0884	2.70e-02	1.10e-02	1.05e-02	1.04e-02	1.04e-02
0.0442	2.28e-02	3.99e-03	2.75e-03	2.61e-03	2.59e-03
0.0221	2.21e-02	2.91e-03	9.92e-04	6.85e-04	6.52e-04
0.0110	2.19e-02	2.79e-03	7.22e-04	2.46e-04	1.71e-04

Table 12: Errors in $\|\cdot\|_{L^2(Q)}$ of the Galerkin–Bubnov FEM (40) with the approximate right-hand side $\Pi_h^{\mathcal{RT},1} \underline{j} \in S^1(\mathcal{T}_\alpha^t) \otimes \mathcal{RT}^0(\mathcal{T}_\nu^x)$ for $T = \sqrt{2}$, the unit square Ω and \underline{A} in (45).

We observe unconditional stability in Table 9, Table 10, Table 11, Table 12, i.e. no CFL condition is needed. This is the main difference between the results in this subsection and the results of Subsection 7.1, where for stability, a CFL condition is required.

Besides the stability issue, the errors in Table 9, Table 10, Table 11, Table 12 are comparable with the errors of the previous Subsection 7.1 regarding the projection of the right-hand side. Thus, the approximation $\Pi_h^0 \underline{j} \in S^0(\mathcal{T}_\alpha^t) \otimes S_2^0(\mathcal{T}_\nu^x)$ of \underline{j} is good enough to get first-order convergence in $|\cdot|_{H^{\text{curl};1}(Q)}$, see Table 9. In Table 12, we again see that the better approximation $\Pi_h^{\mathcal{RT},1} \underline{j} \in S^1(\mathcal{T}_\alpha^t) \otimes \mathcal{RT}^0(\mathcal{T}_\nu^x)$ of \underline{j} is needed for optimal convergence rates in $\|\cdot\|_{L^2(Q)}$.

8 Conclusion

In this paper, we presented two conforming space-time finite element methods for the vectorial wave equation. First, we stated a variational formulation with different trial and test spaces. Its conforming discretization with piecewise multilinear functions leads to a Galerkin–Petrov method, which is only conditionally stable, i.e. a CFL condition is required. For a particular choice of spatial meshes, we stated the CFL condition, where numerical examples showed its sharpness. Second, to tackle the problem of a CFL condition, we introduced a variational formulation for the vectorial wave equation with equal trial and test spaces using the modified Hilbert transformation \mathcal{H}_T . We gave a rigorous derivation of this variational setting. A conforming discretization with piecewise multilinear functions of this new variational approach results in a space-time Galerkin–Bubnov method. All numerical examples showed the unconditional stability of this conforming space-time method. Further, we investigated the influence of projections of the right-hand side on the convergence. In numerical examples for both the Galerkin–Petrov method and the Galerkin–Bubnov method, we observed only first-order convergence in $\|\cdot\|_{L^2(Q)}$ when the right-hand side was projected onto piecewise constants. On the other side, second-order convergence was obtained when the right-hand side was projected onto piecewise linear functions in time and lowest-order Raviart–Thomas functions in space.

For both presented conforming space-time approaches, a generalization to piecewise polynomials of higher-order is possible, see [16]. Further, the fast solvers [23, 37, 38] for the resulting linear systems, where some allow for time parallelization, are also applicable. In addition, other time-dependent problems in electromagnetics can be handled with the presented variational frameworks, which are topics of future work, see e.g. [16].

References

- [1] ABEDI, R., AND MUDALIAR, S. An asynchronous spacetime discontinuous Galerkin finite element method for time domain electromagnetics. *J. Comput. Phys.* 351 (2017), 121–144.
- [2] ARNOLD, D. N., FALK, R. S., AND WINTHER, R. Finite element exterior calculus, homological techniques, and applications. *Acta Numer.* 15 (2006), 1–155.
- [3] ASSOUS, F., CIARLET, P., AND LABRUNIE, S. *Mathematical foundations of computational electromagnetism*, vol. 198 of *Applied Mathematical Sciences*. Springer, Cham, 2018.
- [4] BAI, X., AND RUI, H. A second-order space-time accurate scheme for Maxwell’s equations in a Cole–Cole dispersive medium. *Engineering with Computers* 38, 6 (2022), 5153–5172.
- [5] BOSSAVIT, A. Solving Maxwell equations in a closed cavity, and the question of ‘spurious modes’. *IEEE Transactions on Magnetics* 26, 2 (1990), 702–705.
- [6] CHARI, M., KONRAD, A., PALMO, M., AND D’ANGELO, J. Three-dimensional vector potential analysis for machine field problems. *IEEE Transactions on Magnetics* 18, 2 (1982), 436–446.
- [7] CHAUHAN, A., FERROUILLAT, P., RAMDANE, B., MARÉCHAL, Y., AND MEUNIER, G. A review on methods to simulate three dimensional rotating electrical machine in magnetic vector potential formulation using edge finite element method under sliding surface principle. *International Journal of Numerical Modelling: Electronic Networks, Devices and Fields* 35, 1 (2021), e2925.
- [8] CRAWFORD, Z. D., LI, J., CHRISTLIEB, A., AND SHANKER, B. Unconditionally stable time stepping method for mixed finite element Maxwell solvers. *Progress In Electromagnetics Research C* 103 (2020), 17 – 30.
- [9] DAVIS, T. A. Algorithm 832: UMFPACK V4.3 – an unsymmetric-pattern multifrontal method. *ACM Trans. Math. Softw.* 30, 2 (2004), 196–199.
- [10] DÖRFLER, W., FINDEISEN, S., AND WIENERS, C. Space-time discontinuous Galerkin discretizations for linear first-order hyperbolic evolution systems. *Comput. Methods Appl. Math.* 16, 3 (2016), 409–428.
- [11] EGGER, H., KRETZSCHMAR, F., SCHNEPP, S. M., AND WEILAND, T. A space-time discontinuous Galerkin Trefftz method for time dependent Maxwell’s equations. *SIAM J. Sci. Comput.* 37, 5 (2015), B689–B711.
- [12] ERN, A., AND GUERMOND, J.-L. *Finite elements I—Approximation and interpolation*, vol. 72 of *Texts in Applied Mathematics*. Springer, Cham, 2021.
- [13] ERN, A., AND GUERMOND, J.-L. *Finite elements II—Galerkin Approximation, Elliptic and Mixed PDEs*, vol. 73 of *Texts in Applied Mathematics*. Springer, Cham, 2021.

- [14] GIRAULT, V., AND RAVIART, P.-A. *Finite element methods for Navier-Stokes equations*, vol. 5 of *Springer Series in Computational Mathematics*. Springer-Verlag, Berlin, 1986.
- [15] HAUSER, J. I. M. *Space-Time Methods for Maxwell's Equations - Solving the Vectorial Wave Equation*. PhD thesis, Graz University of Technology, 2021.
- [16] HAUSER, J. I. M. Space-Time FEM for the Vectorial Wave Equation under Consideration of Ohm's Law. [math.NA] arXiv:2301.03381, arXiv.org, 2023.
- [17] HAUSER, J. I. M., KURZ, S., AND STEINBACH, O. Space-time finite element methods for the vectorial wave equation. *In preparation*.
- [18] HOCHBRUCK, M., AND STURM, A. Upwind discontinuous Galerkin space discretization and locally implicit time integration for linear Maxwell's equations. *Math. Comp.* 88, 317 (2019), 1121–1153.
- [19] IONEL, D. M., AND POPESCU, M. Finite-element surrogate model for electric machines with revolving field-application to IPM motors. *IEEE Transactions on Industry Applications* 46, 6 (2010), 2424 – 2433.
- [20] JACKSON, J. D., AND OKUN, L. B. Historical roots of gauge invariance. *Rev. Modern Phys.* 73, 3 (2001), 663–680.
- [21] JIN, J. *The finite element method in electromagnetics*, second ed. Wiley-Interscience, New York, 2002.
- [22] LANG, S. *Differential and Riemannian manifolds*, third ed., vol. 160 of *Graduate Texts in Mathematics*. Springer-Verlag, New York, 1995.
- [23] LANGER, U., AND ZANK, M. Efficient direct space-time finite element solvers for parabolic initial-boundary value problems in anisotropic Sobolev spaces. *SIAM J. Sci. Comput.* 43, 4 (2021), A2714–A2736.
- [24] LILIENTHAL, M., SCHNEPP, S. M., AND WEILAND, T. Non-dissipative space-time hp -discontinuous Galerkin method for the time-dependent Maxwell equations. *J. Comput. Phys.* 275 (2014), 589–607.
- [25] LOGG, A., MARDAL, K.-A., AND WELLS, G., Eds. *Automated solution of differential equations by the finite element method. The FEniCS book*, vol. 84 of *Lect. Notes Comput. Sci. Eng.* Berlin: Springer, 2012.
- [26] LÖSCHER, R., STEINBACH, O., AND ZANK, M. An unconditionally stable space-time finite element method for the wave equation. *In preparation*.
- [27] LÖSCHER, R., STEINBACH, O., AND ZANK, M. Numerical results for an unconditionally stable space-time finite element method for the wave equation. In *Domain Decomposition Methods in Science and Engineering XXVI*, vol. 145 of *Lect. Notes Comput. Sci. Eng.* Springer, Cham, 2022, pp. 587–594.
- [28] MONK, P. *Finite element methods for Maxwell's equations*. Numer. Math. Sci. Comput. Oxford: Oxford University Press, 2003.

- [29] SCHÖBERL, J. NETGEN: An advancing front 2d/3d-mesh generator based on abstract rules. *Comput. Vis. Sci.* 1, 1 (1997), 41–52.
- [30] STEINBACH, O., AND MISSONI, A. A note on a modified Hilbert transform. *Applicable Analysis* (2022), 1–8.
- [31] STEINBACH, O., AND ZANK, M. Coercive space-time finite element methods for initial boundary value problems. *Electron. Trans. Numer. Anal.* 52 (2020), 154–194.
- [32] STEINBACH, O., AND ZANK, M. A note on the efficient evaluation of a modified Hilbert transformation. *J. Numer. Math.* 29, 1 (2021), 47–61.
- [33] STERN, A., TONG, Y., DESBRUN, M., AND MARSDEN, J. E. Geometric computational electrodynamics with variational integrators and discrete differential forms. In *Geometry, mechanics, and dynamics*, vol. 73 of *Fields Inst. Commun.* Springer, New York, 2015, pp. 437–475.
- [34] TIEGNA, H., AMARA, Y., AND BARAKAT, G. Overview of analytical models of permanent magnet electrical machines for analysis and design purposes. *Mathematics and Computers in Simulation* 90 (2013), 162–177.
- [35] XIE, J., LIANG, D., AND ZHANG, Z. Energy-preserving local mesh-refined splitting FDTD schemes for two dimensional Maxwell’s equations. *J. Comput. Phys.* 425 (2021), Paper No. 109896, 29.
- [36] XIE, Z., WANG, B., AND ZHANG, Z. Space-time discontinuous Galerkin method for Maxwell’s equations. *Commun. Comput. Phys.* 14, 4 (2013), 916–939.
- [37] ZANK, M. Efficient direct space-time finite element solvers for the wave equation in second-order formulation. *In preparation*.
- [38] ZANK, M. High-order discretisations and efficient direct space-time finite element solvers for parabolic initial-boundary value problems. *To appear in Proceedings of Spectral and High Order Methods for Partial Differential Equations ICOSAHOM 2020+1*.
- [39] ZANK, M. *Inf-Sup Stable Space-Time Methods for Time-Dependent Partial Differential Equations*, vol. 36 of *Monographic Series TU Graz: Computation in Engineering and Science*. 2020.
- [40] ZANK, M. An exact realization of a modified Hilbert transformation for space-time methods for parabolic evolution equations. *Comput. Methods Appl. Math.* 21, 2 (2021), 479–496.
- [41] ZANK, M. Integral representations and quadrature schemes for the modified Hilbert transformation. *Computational Methods in Applied Mathematics* (2022).